THESIS FOR THE DEGREE OF LICENTIATE OF ENGINEERING

Ultra-wideband feed design and characterization for next generation radio telescopes

JONAS FLYGARE

Department of Space, Earth and Environment
Onsala Space Observatory
CHALMERS UNIVERSITY OF TECHNOLOGY
Göteborg, Sweden 2018

Ultra-wideband feed design and characterization for next generation radio telescopes
JONAS FLYGARE

Email: jonas.flygare@chalmers.se or jonas.b.flygare@gmail.com

Department of Space, Earth and Environment
Onsala Space Observatory
Chalmers University of Technology
SE-412 96 Göteborg
Sweden
Telephone: +46 (0)31-772 1000

Cover:
Top-left: The SKA Band 1 QRFH feed package, image credit: Chalmers / Johan Bodell; Top-right: Onsala twin telescopes, and Onsala 25 m telescope, image credit: Roger Hammargren, OSO. Bottom-left: SKA Band 1 QRFH feed package installed on MeerKAT for qualification tests, image credit: George Smit, SARAO; Bottom-right: BRAND EVN prototype QRFH.

Chalmers Reproservice
Göteborg, Sweden 2018

Ultra-wideband feed design and characterization for next generation radio telescopes
JONAS FLYGARE
Department of Space, Earth and Environment
Onsala Space Observatory
Chalmers University of Technology

Abstract

Radio telescopes are used as tools for observations in both radio astronomy and geodesy. To observe the weak sources in space, highly sensitive receivers headed by optimized reflector feeds are needed. Wideband and ultra-wideband (UWB) receiver systems enable large continuous frequency bandwidth and reduce the number of receivers that are needed. Therefore, they are attractive for the next generation of large reflector arrays such as the Square Kilometre Array (SKA) and the Next Generation Very Large Array (ngVLA). To achieve highly sensitive wideband and UWB performance with reflector feeds, a near-constant beamwidth and good impedance match are required over large frequency bands. The quad-ridge flared horn (QRFH) is a robust and popular UWB feed technology for this purpose. Typically, the QRFH achieve good performance up to 6:1 bandwidth and are designed for high aperture efficiency. However, due to the very small noise contributions of today's low-noise amplifiers (LNA), it is becoming more relevant to design specifically for high sensitivity. A drawback in existing state-of-the-art QRFH designs, is that they suffer from narrowing beamwidth as the frequency increases over the bandwidth. To meet the demand for high sensitivity observations over large bandwidths, these challenges need to be addressed.

In this thesis, the spline-defined QRFH design for the room temperature SKA Band 1 feed package over 350–1050 MHz is presented. The QRFH spline-profile is optimized for high sensitivity over the 3:1 bandwidth for the SKA reflector dish. The thesis also introduces a low-profiled dielectric load at the center of a QRFH design for 10:1 bandwidth for the BRAND project. The dielectric load improves the beamwidth performance over the 1.5–15.5 GHz frequency band, while keeping the complexity of the QRFH concept low. Both of the approaches that are introduced here are applicable for any future QRFH design, and are therefore relevant for the community in the hunt for high sensitivity observations.

Keywords: Ultra-wideband antennas, reflector feed, quad-ridge flared horn, spline-defined, decade bandwidth, dielectric loading, radio astronomy, geodesy, square kilometre array

Occupy Mars

Preface

The work included in this thesis has been conducted at the Onsala Space Observatory, Chalmers University of Technology, Sweden. Part of the project included in this publication has been funded by Swedish VR Research Infrastructures Planning Grant for Swedish contributions to the SKA radio-telescope in its pre-construction phase. Part of the project included in this publication has received funding from the European Union's Horizon 2020 research and innovation programme under grant agreement No 730562 [RadioNet].

Acknowledgement

Thank you to all the people who have supported me throughout this work. Many thanks to my main supervisor Rüdiger Haas and my co-supervisors Miroslav Pantaleev and Jian Yang for all their wisdom and help. A special thanks to Miroslav for trusting me to do the SKA Band 1 feed design and giving me this great opportunity from the start. Big thanks to my examiner John Conway for continuously keeping me at the observatory all these years.

Infinite love and gratitude to Mom and Dad, you are always there and supporting me through whatever the situation is. Thanks to friends and family for all the joy you spread in my life. Thanks to the many people around the world that filled the last few years with so much excitement and knowledge for me. All the travels would not have been what they were without you guys, and the sled-dogs of Svalbard. Shout-out to the antenna family on the 7th floor, and the fantastic earth-to-space crew.

Last but not least, a big hug to the people of the electronics lab and mechanical workshop at the observatory. It is truly a pleasure to work with you in the roller-coaster environment of Onsala. You have taught me countless things about everything from coaxial cables to how you should approach life in the strangest of situations.

Jonas Flygare
Göteborg, November 2018

Fig. 1: Onsala, May 2018. Image credit: Chalmers / Johan Bodell.

Nomenclature

ASH	Analytic-Spline-Hybrid
ATA	Allen Telescope Array
BRAND	BRoad-bAND
EVN	European VLBI Network
FoM	Figure-of-merit
GA	Genetic algorithm
HCTF	Hot-cold test facility
HPBW	Half-power beamwidth (3 dB)
LNA	Low-noise amplifier
MeerKAT	"More" Karoo Array Telescope
ngVLA	Next Generation Very Large Array
OTT	Onsala twin telescope
PO	Physical optics
PSO	Particle swarm optimization
PTD	Physical theory of diffraction
PTFE	Polytetrafluoroethylene (Teflon)
QRFH	Quad-ridge flared horn
Rx	Receiver
SEFD	System equivalent flux density
SKA	Square Kilometre Array
SNR	Signal-to-noise ratio
Tx	Transmitter
UWB	Ultra-wideband
VGOS	VLBI Global Observing System
VLBI	Very Long Baseline Interferometry

Thesis

This thesis is based on the work in the following included papers:

Paper A **J. Flygare**, B. Billade, M. Dahlgren, M. Pantaleev, J. Dahlström, B. Wästberg, G. Hovey, R. Hellyer, R. Messing, B. Veidt, G. Lacy, and M. Islam, "Beam pattern measurement on offset Gregorian reflector mounted with a wideband room temperature receiver for the Square Kilometre Array", in *Proc. IEEE Int. Symp. Antennas Propag. (APSURSI 2018)*, Boston, MA, USA, Jul. 2018

Paper B **J. Flygare**, A. Peens-Hough, L. Helldner, M. Dahlgren, G. Smit, P. Kotze, R. Wingdén, T. D. Carozzi, U. Kylenfall, L. Pettersson, and M. Pantaleev, "Sensitivity simulation and measurement of the SKA Band 1 wideband feed package on MeerKAT", in *Submitted Oct. 2018 to 13th Euro. Conf. Antennas Propag. (EuCAP 2019)*

Paper C **J. Flygare**, M. Pantaleev, and S. Olvhammar, "BRAND: Ultra-Wideband Feed Development for the European VLBI Network - A Dielectrically Loaded Decade Bandwidth Quad-Ridge Flared Horn", in *Proc. 12th Euro. Conf. Antennas Propag. (EuCAP 2018)*, London, UK, Apr. 2018

Paper D **J. Flygare** and M. Pantaleev, "Dielectrically Loaded Quad-Ridge Flared Horn for Beamwidth Control over Decade Bandwidth - Optimization, Manufacture, and Measurement", *Submitted Nov. 2018 to IEEE Trans. Antennas Propag.*,

Below follows other publications by the author:

B. Dong, J. Yang, J. Dahlström, **J. Flygare**, M. Pantaleev, and B. Billade, "Optimization and Realization of Quadruple-ridge Flared Horn with New Spline-defined Profiles as a High-efficiency Feed for Reflectors over 4.6 - 24 GHz", *IEEE Trans. Antennas Propag., Accepted for publication Sep. 2018*,

J. Flygare, M. Pantaleev, J. Conway, M. Lindqvist, L. Helldner, M. Dahlgren, and P. Forkman, "Ultra-wideband feed systems for the EVN and SKA - evaluated for VGOS", in *Proc. 10th General Meeting, International VLBI Service for Geodesy and Astrometry (IVS 2018)*, Longyearbyen, Svalbard, Norway, Jun. 2018

J. Flygare, M. Pantaleev, J. Conway, and M. Lindqvist, "Design trade-offs in feed systems for ultra-wideband VLBI observations", in *Proc. 10th General Meeting, International VLBI Service for Geodesy and Astrometry (IVS 2018)*, Longyearbyen, Svalbard, Norway, Jun. 2018

T. Carozzi and **J. Flygare**, "Enhancing SKA Band 1 Polarimetry by Using Two Different Feed Rotations", in *2nd URSI AT-RASC*, Gran Canaria, Spain, Jun. 2018

B. Dong, J. Yang, M. Pantaleev, **J. Flygare**, and B. Billade, "Design of an Asymmetrical Quadruple-ridge Flared Horn Feed : a Solution to Eliminate Polarization Discrepancy in the Offset Reflecting Systems", in *Proc. 12th Euro. Conf. Antennas Propag. (EuCAP 2018)*, London, UK, Apr. 2018

S. Weinreb, H. Mani, W. Zhong, **J. Flygare**, B. Billade, A. Akgiray, and L. Dong, "Cryogenic 1.2 to 116 GHz Receiver for Large Arrays", in *Proc. 12th Euro. Conf. Antennas Propag. (EuCAP 2018)*, London, UK, Apr. 2018

J. Flygare, B. Billade, M. Dahlgren, B. Wästberg, and M. Pantaleev, "Integrated calibration noise coupler for room temperature SKA Band 1 feed system", in *Proc. IEEE Int. Symp. Antennas Propag. (APSURSI 2017)*, San Diego, CA, USA, Jul. 2017, pp. 777–778

J. Flygare, M. Pantaleev, B. Billade, M. Dahlgren, L. Helldner, and R. Haas, "Sensitivity and Antenna Noise Temperature Analysis of the Feed System for the Onsala Twin Telescopes", in *Proc. 23rd Working Meeting of the Euro. Very Long Baseline Interferometry Group for Geodesy and Astrometry (EVGA 2017)*, Gothenburg, Sweden, May 2017, pp. 10–14. [Online]. Available: `https://research.chalmers.se/en/publication/253461`

M. Pantaleev, L. Helldner, R. Haas, K. Johansson, L. Petterson, J. Dahlström, M. Dahlgren, U. Kylenfall, B. Billade, and **J. Flygare**, "Design, Implementation and Tests of the Signal Chain for the Twin Telescopes at Onsala Space Observatory", in *Proc. 23rd Working Meeting of the Euro. Very Long Baseline Interferometry Group for Geodesy and Astrometry (EVGA 2017)*, Gothenburg, Sweden, May 2017, pp. 15–19. [Online]. Available: `https://research.chalmers.se/en/publication/253548`

G. Tuccari, W. Alef, M. Pantaleev, **J. Flygare**, J. A. López Pérez, J. A. López Fernández, G. Schonderbeek, and V. Bezrukos, "BRAND: A very wide-band receiver for the EVN", in *Proc. 23rd Working Meeting of the Euro. Very Long Baseline Interferometry Group for Geodesy and Astrometry (EVGA 2017)*, Gothenburg, Sweden, May 2017, pp. 81–83

J. Yang, **J. Flygare**, M. Pantaleev, and B. Billade, "Development of quadruple-ridge flared horn with spline-defined profile for band B of the Wide Band Single Pixel Feed (WBSPF) advanced instrumentation programme for SKA", in *Proc. IEEE Int. Symp. Antennas Propag.*, Fajardo, Puerto Rico: IEEE, Jul. 2016, pp. 1345–1346, ISBN: 9781509028863. DOI: `10.1109/APS.2016.7696380`. [Online]. Available: `http://ieeexplore.ieee.org/document/7696380/`

B. Billade, **J. Flygare**, M. Dahlgren, B. Wästberg, and M. Pantaleev, "A wide-band feed system for SKA band 1 covering frequencies from 350 - 1050 MHz", in *Proc. 10th*

Euro. Conf. Antennas Propag. (EuCAP 2016), Davos, Switzerland, Apr. 2016, ISBN: 9788890701863. DOI: 10.1109/EuCAP.2016.7481794

G. W. Walker, E. Kalinauskaite, D. N. McCarthy, N. A. Trappe, A. Murphy, L. Helldner, M. G. Pantaleev, and **J. Flygare**, "Optical design and verification of a 4mm receiver for the 20m telescope at Onsala Space Observatory", in *Proceedings Volume 9914, Millimeter, Submillimeter, and Far-Infrared Detectors and Instrumentation for Astronomy VIII; 99142V, 26 June - 1 July*, vol. 9914, Edinburgh, United Kingdom: SPIE, 2016, ISBN: 9781510602076. DOI: 10.1117/12.2232576. [Online]. Available: http://proceedings.spiedigitallibrary.org/proceeding.aspx?doi=10.1117/12.2232576

A. Algaba Brazalez, **J. Flygare**, J. Yang, V. Vassilev, M. Baquero-Escudero, and P.-S. Kildal, "Design of F-Band Transition from Microstrip to Ridge Gap Waveguide Including Monte Carlo Assembly Tolerance Analysis", *IEEE Trans. Microw. Theory Techn.* vol. 64, no. 4 Apr. 2016, pp. 1245–1254, Apr. 2016, ISSN: 00189480. DOI: 10.1109/TMTT.2016.2535334

V. Belitsky, I. Lapkin, M. Fredrixon, E. Sundin, L. Helldner, L. Pettersson, S. Ferm, M. Pantaleev, B. Billade, P. Bergman, A. O. H. Olofsson, M. S. Lerner, M. Strandberg, M. Whale, A. Pavolotsky, **J. Flygare**, H. Olofsson, and J. Conway, "A new 3 mm band receiver for the Onsala 20 m antenna", *Astronomy & Astrophysics* vol. 580 2015, pp. 1–6, 2015, ISSN: 14320746. DOI: 10.1051/0004-6361/201425573. [Online]. Available: https://doi.org/10.1051/0004-6361/201425573

Contents

PART I

Introductory Chapters

CHAPTER 1

Introduction

In 1928, Bell Laboratories in Holmdel, New Jersey wanted to study transatlantic radio frequency interference (RFI) for short-wave communications. The newly graduated engineer Karl G. Jansky, with a degree in physics, was hired to do the job. Jansky designed an antenna at 20.5 MHz ($\lambda = 14.5$ m) mounted on a large rotational platform that used tires from a model T-ford to go around. Jansky studied the radio waves in all directions for quite some time and found that the most common noise the antenna picked up was the electromagnetic waves generated from accelerating charges in thunderstorms [1]. But he also found a weaker signal that came about and disappeared once a day. Jansky was curious about the origin of this signal and continued to study it for several months. A qualified guess was that the signal came from the Sun, however the time period was slightly less than 24 hours. Could it be from something outside our solar-system? The conclusion was that the signal came from the center of our Milky Way galaxy where the star constellation Sagittarius is located. Jansky had unintentionally performed one of the first ever radio astronomical observations and it was published in 1932. He was very keen on continuing his work within this newly discovered field, however Bell Laboratories had other plans for him. Sadly he was moved to other assignments within the company, and died at the age of 44. The field of radio astronomy did however live on and today, the projects around the world involving radio telescopes probably reaches far beyond the imagination of Jansky.

To honor Jansky, the flux density strength of observed radio sources has been given the unit with his name (Jy). Consequently, the sensitivity of the instruments needed to study these faint sources far away, are given in the same unit. System equivalent flux density (SEFD) is a figure-of-merit for radio telescopes with its receiver system [2]. A low SEFD number implies a high signal-to-noise ratio (SNR) and therefore a highly sensitive telescope for observation. The radio sources in space vary vastly in strength where a flux density above 1 Jy would be considered relatively strong but also quite uncommon. For comparison, a cell-phone's flux density measured from a distance of 1 km at 1.8 GHz corresponds to roughly $1.1 \cdot 10^8$ Jy. However, most astronomical sources are much weaker than 1 Jy, and can be in the range of micro-Jy (μJy, 10^{-6}). To study these sources, scientists need highly optimized radio telescope equipment.

Radio telescopes are most commonly designed as large mechanically steerable reflectors with a pencil-beam [1]. The reflector collects incoming radiation proportional to the area and focuses it to the focal point where the receiving system is located. There are other forms of telescopes such as synthesized aperture arrays with a large field of view [3] or fixed giant reflectors that can steer the beam by suspended movable receiving systems [4], [5].

Fig. 1.1: Onsala's two 13.2 m twin telescope reflectors on the left and the 25 m telescope on the right. Image credit: Roger Hammargren, OSO.

Synthesized large apertures can be formed by telescopes through interferometry. By using telescopes separated with large distances, the technique of Very-Long Baseline Interferometry (VLBI) can increase the observational resolution drastically [2]. Another application of the VLBI technique is to use known sources, that are stable in its position relative to earth, as reference directions. If we have several of these telescopes, spread across the globe, and looking at the same source, we can very accurately determine the separation between them. This is done by high-precision timing of when the signal was received at each telescope, using atomic clocks. In fact, this geodetic VLBI technique is the only space-based technique that can determine all five earth orientation parameters (EOP), and give us a direct connection between the space-based and the Earth-fixed reference frame [6]. This gives us knowledge about the irregularities in the rotation of the Earth - Universal time, and the direction of the earth rotation vector. The next generation of space-geodetic VLBI is realized through the VLBI Global Observing System (VGOS) [7],[8]. The idea is to build a rather standardized observations system of 12–13 m reflector telescopes at the VLBI stations around the world, to continuously observe and provide geodynamical data – 24 hours a day. The location precision is expected to be in the order of 1 mm. One of the most recently inaugurated VGOS stations is the Onsala Twin Telescope (OTT), consisting of two identical reflectors, see Fig. 1.1, that can achieve continuous observation of sources. The continuos coverage is achieved by moving the non-observing telescope to a new source while the other is actively observing [9]. The receiver systems of VGOS need a very wide frequency bandwidth to observe sources that emit radiation at many different wavelengths.

The sensitivity for observations with a reflector telescope system is dependent on several factors. The larger the receiving area is, the more incoming radio waves it can collect. How efficiently this is done is one key to a sensitive system. Another very important factor is that the receiver itself must be designed as a low-noise, well calibrated, electronics system which is headed by the feed antenna. How optimal the feed converts the

incoming radio waves into electric signals is crucial. For some narrow frequency feeds this has been done with high efficiency, and therefore high sensitivity [10]. For a wideband feed, high sensitivity over the large bandwidth is a challenge due to less consistent illumination from the feed beam pattern over frequency. Typically the impedance match is difficult for very wide bandwidths. The receiving SNR for detection will increase proportional to the square root of available bandwidth and integration time. A single wideband feed system can also cover a frequency range that otherwise require multiple narrowband systems. Generally, a limited space is available in each telescope for the receiver systems and each of these systems are cryogenically cooled which requires moving parts. For a set of several hundreds of telescopes, as in the case of a large interferometric array, multiple narrowband systems increase the cost and maintenance time substantially. The complexity allowed for the telescope architecture, with an increasing number of receiving systems, eventually limits this approach. By using a sensitive wideband system instead we can reduce manufacturing and maintenance cost, power consumption and the available space needed to install the receiver. Highly optimized wideband feeds and receiver systems are therefore very advantageous, especially for large telescope arrays with relatively low f/D reflectors such as: the Next Generation Very Large Array (ngVLA) [11]; the Allen Telescope Array (ATA) [12]; the MeerKAT ("More" Karoo Array Telescope) [13]; and the Square Kilometre Array (SKA) [14]. The SKA project will cover the frequency range 350 MHz to 15.3 GHz with the 133 SKA-MID reflectors, divided into five frequency bands. Eventually the 64 MeerKAT reflectors will be included as a part of the SKA-MID. The science goals set for the SKA are truly inspiring, aiming to study: the first galaxies of the universe and their evolution; dark energy; cosmic magnetism; gravitational waves; and the protoplanetary disks, to name just a few. Once finalized, the SKA observational sensitivity will be unprecedented over this frequency range and enable new scientific discoveries.

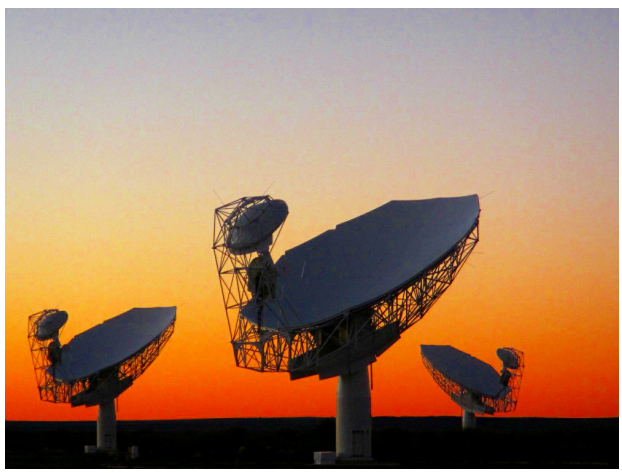

Fig. 1.2: Three of the 64 offset Gregorian reflectors of MeerKAT, each with a 13.5 m diameter, located in the Karoo desert, South Africa. Image credit: Leif Helldner, OSO.

The reason to use large telescope arrays is the enormous gain in observational sensitivity compared to what single telescopes (of realistic diameter size) can achieve. As mentioned, most radio sources are very weak, so to be able to study these sources with a realistic integration time we need to increase the sensitivity. The sensitivity increases with the number of telescopes (collecting area) but also with the frequency bandwidth available in the receivers. There is also a benefit to allow for observation over a wider range of frequencies simultaneously. As mentioned, a key challenge with wideband receivers is to illuminate the telescope reflector constant over a large bandwidth with a single feed. Another reason has been the difficulty of building well-matched low-noise amplifiers (LNA) over a large bandwidth. In recent years, the LNA technology has matured immensely and can deliver very low noise for even decade frequency bandwidth [15], [16], [17], [18]. To utilize this bandwidth, highly optimized and well impedance-matched wideband and ultra-wideband (UWB) feeds are required. An impressive amount of work the last two decades has been put in to development of different kinds of UWB feeds for radio telescopes. Examples are the: Antonio Feed [12]; Eleven-Feed [19], [20]; Quasi-Self-Complementary Feed (QSC) [21] and the Quad-ridge Flared Horn (QRFH) [22], [23]. The QRFH has been well-explored in [24] and [25] as well.

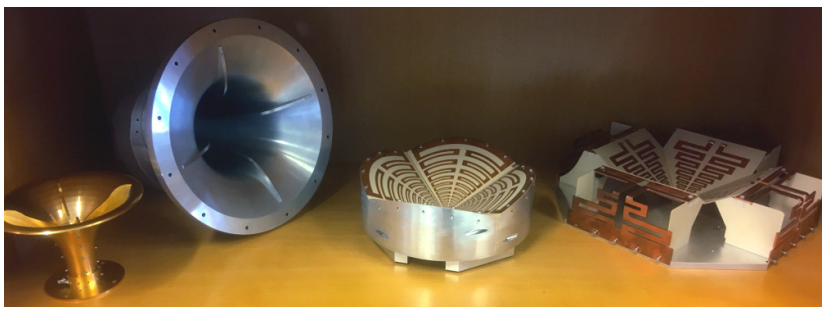

Fig. 1.3: UWB QRFHs and Eleven-Feeds for different frequencies and reflector geometries.

The QRFH is a pure metal, flared-out section of a quad-ridge waveguide with low loss and robust structure. Due to the ridge structure, it can achieve dual-linear polarization in a compact form. There is no need for an orthomode transducer (OMT). QRFHs can be designed for single-ended feeding which only requires one LNA per polarization, keeping the complexity low. Typically with a 50 Ω interface, the QRFH can achieve input reflection coefficient less than -10 dB for 6:1 bandwidth [22]. The waveguide properties give the QRFH a sharp lower cut-off frequency which mitigates radio frequency interference (RFI). The shape and structure is usually straightforward to manufacture without complex or expensive methods for assembly. Because of the compact design, robustness and single-ended feeding the integration in a cryostat dewar is simple. As the radio community wants to push the observational bandwidths above a decade in frequency, there is a need to push the QRFH operational bandwidth. To do this without jeopardizing the simple concept of the QRFH, is therefore a valuable approach.

1.1 Aim of the thesis

In this thesis, new development is presented for ultra-wideband QRFH reflector feeds, mainly designed as a part of larger projects in SKA and the European VLBI Network (EVN). The QRFH technology is improved with two specific concepts in mind: 1) Design for high sensitivity over 3:1 bandwidth with spline-defined horn and ridge profiles; 2) Improve phase efficiency and beamwidth-control over decade bandwidth with a simple dielectric load. Design, manufacture and measurement of the UWB QRFH is discussed on the feed level but also the receiver system performance of these designs on reflector telescopes. Key system parameters are mentioned where the most important is receiver sensitivity. A discussion of the QRFH design approach and system evaluation tools is also included. The key mindset throughout this work is practical implementation of the designs for real applications. This is something the author feels strongly about as the field borderlines pure research and product realization. The work presented herein has been conducted at the Onsala Space Observatory, Chalmers University of Technology, Sweden.

The SKA Band 1 ranges over 350–1050 MHz and is the lowest frequency band on the SKA-MID reflectors. The wide bandwidth is covered by a complete room temperature feed package with high sensitivity. The work presented in this thesis has led to the design and characterization of the spline-defined 3:1 QRFH at the front of the Band 1 feed package (Paper A, Paper B).

The RadioNet sponsored EU Horizon 2020 project BRoad-bAND (BRAND) EVN aims to cover L-,S-,C-,X-, and Ku-band with one single receiver [26]. BRAND has the goal to offer a complete astronomy receiver package for applicable telescopes, and be compatible with the VGOS frequency range 2–14 GHz. The work in this thesis has led to the dielectrically loaded decade bandwidth QRFH over 1.5–15.5 GHz for the BRAND project (Paper C, Paper D).

1.2 Structure of the thesis

The thesis chapters 1–4 introduce the field together with the work presented in the appended papers. Chapter 1 is a short overview of radio astronomy and space-geodesy together with the field of radio telescopes and feed design. In Chapter 2 the most relevant theory to evaluate a reflector feed system is introduced: an overview of the antenna noise temperature and sensitivity calculation framework. In Chapter 3 the QRFH concept for UWB design is introduced and what improvements have been done. Finally, Chapter 4 gives a brief summary of the included papers and the future possibilities derived off of this work.

CHAPTER 2

Reflector Feed Characterization

To characterize feed designs, the sensitivity and other system characteristics of the proposed receiver for a certain reflector geometry has to be calculated. In this chapter a brief overview of the typical framework used for that characterization is given. The calculations are give for radio telescopes equipped with single-pixel feed receivers. General electromagnetic and antenna theory is assumed, otherwise relevant sources are: [1], [2], [27], [28], [29], [30]. The nomenclature and syntax in the thesis can deviate from references. The antenna applications presented herein are in receiver configuration, however in the discussion the terminology may sometimes describe the situation as if the antennas were transmitting. This is a common, intuitive approach when spill-over and illumination from feed horns are discussed.

2.1 Reflector geometry

Feed design for reflector-type radio telescopes is dependent on the geometry of the reflector. Typically, the reflector has two orthogonal polarizations defined, which require a dual-polarized feed to illuminate. Other parameters such as reflector size, edge-taper, blockage, and possible sub-reflector configuration are all key parameters influencing the optimization approach, choice of feed type and achievable performance. In Fig. 2.1 a standard unshaped prime-focus parabolic reflector is illustrated. The available reflector area is calculated

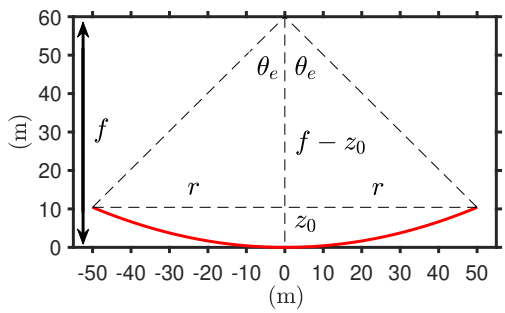

Fig. 2.1: Schematics of an unshaped prime-focus axisymmetric parabolic reflector, θ_e is the half-subtended angle from the focal point.

as $A_{\text{phy}} = \pi D^2/4$ where the diameter is $D = 2r$. With basic trigonometry, the half-subtended angle θ_e can be expressed in terms of the focal length, f, to diameter ratio, f/D, according to

$$\begin{aligned}\tan\theta_e &= \frac{r}{f - z_0} = \left\{ z_0 = \frac{r^2}{4f} \right\} = \frac{r}{f - \frac{r^2}{4f}} \\ &= \left\{ r = \frac{D}{2} \right\} = \frac{\frac{D}{2}}{f - \frac{D^2}{16f}} = \frac{1}{2} \frac{\frac{f}{D}}{(\frac{f}{D})^2 - \frac{1}{16}}. \end{aligned} \tag{2.1}$$

The half-angle identity for arctan

$$\tan\frac{x}{2} = \frac{\sin x}{1 + \cos x} \Rightarrow \arctan x = 2\arctan\frac{x}{1 + \sqrt{1 + x^2}}, \tag{2.2}$$

can be used to simplify (2.1) as

$$\theta_e = 2\arctan\left(\frac{1}{4\frac{f}{D}}\right). \tag{2.3}$$

From (2.3) a correlation is found for large θ_{e} with low f/D and small θ_{e} with high f/D. Typically low f/D implies a more compact feed design, able to produce larger bandwidth and is a popular approach for large telescope arrays. Traditionally, for single dish observations high f/D Cassegrain dual-reflector geometries have been used which require large feeds often limited to octave bandwidths. For feed design, θ_{e} specifies the break-point of where illuminating power becomes spill-over power in the reflector geometry. When designing the feed for a dual-reflector system, the half-subtended angle from the feed towards the sub-reflector is the most relevant.

2.2 Efficiencies

The effective area, A_{eff}, of a reflector is a measure of how well the available reflector area, A_{phy}, is being illuminated. From the main-beam gain, G, effective area is calculated as $A_{\text{eff}} = G\lambda^2/4\pi$. The aperture efficiency, η_{a}, can be calculated from the relation $A_{\text{eff}} = \eta_{\text{loss}}\eta_{\text{a}}A_{\text{phy}}$ where η_{loss} represents all the losses in the reflector system [31]. These losses can be divided into sub-efficiencies including ohmic and dielectric losses, surface error, jitter in pointing, transparency losses in the reflector and blockage. Depending on the reflector structure and system, these can be very different (e.g. offset reflector has no blockage). It is common to give system specifications of a certain aperture efficiency with a calculated margin that accounts for η_{loss}. The aperture efficiency itself can be divided into multiple sub-efficiencies [32]. For a prime-focus reflector η_{a} is calculated (in linear units) according to

$$\eta_{\text{a}} = \eta_{\text{ill}}\eta_{\text{sp}}\eta_{\text{BOR1}}\eta_{\text{pol}}\eta_{\text{ph}}, \tag{2.4}$$

where η_{ill} is the illumination efficiency, η_{sp} is the spill-over efficiency, η_{BOR1} is the BOR1 (azimuth mode) efficiency, η_{pol} is the polarization (cross-polarization) efficiency, and η_{ph}

is the phase efficiency. The phase efficiency η_{ph} is depedent of the feed's location relative to the focal point of the reflector. Ideall the phase center of the feed is near-constant for a high phase efficiency over the full bandwidth. The product of $\eta_{\text{ill}}\eta_{\text{sp}}$ is the trade-off between how well the reflector is illuminated and how much power is lost to spill-over. The optimal edge taper-level at θ_{e} for a system only designed for high η_{a}, can be found as the maximum of $\eta_{\text{ill}}\eta_{\text{sp}}$ as is illustrated in Figure 2.3 of [24]. However, a design optimized for high sensitivity depends on more factors. The total system noise temperature can be dominated by either surrounding brightness temperature or internal receiver temperature, or they can have similar contributions. This will affect what taper that gives the optimal sensitivity when taking the spill-over noise into account that is picked up from the ground. The possibility to *shape* reflector geometries also influences the trade-off as generally a higher η_{a} can be achieved.

2.3 Sensitivity

To study radio sources in space, scientists want to measure the strength of their radiation. The specific intensity I_ν (or brightness) is an intrinsic property of the radiating source. The incoming flux density of most radio sources ($\ll 1$ radian) can be calculated as

$$S_\nu = \iint_{\Omega_{\text{src}}} I_\nu \mathrm{d}\Omega, \tag{2.5}$$

where Ω_{src} is the solid angle subtended by the source. Due to the extremely weak sources studied in astronomy, the flux density is expressed in a small unit: Jansky (1 Jy=10^{-26} W m^{-2} Hz^{-1}). In the Rayleigh-Jeans limit of Planck's law the brightness of a radio source can be expressed as a brightness temperature according to

$$T_{\text{b},\nu} = \frac{I_\nu \lambda^2}{2k_{\text{B}}}, \tag{2.6}$$

where λ is the wavelength and k_{B} the Boltzmann constant. The brightness temperature corresponds to the physical temperature an equivalent blackbody source would need in order to produce the brightness I_ν. Flux density and brightness temperature are therefore proportional as concluded from (2.5) and (2.6). The figure-of-merit (FoM) for a radio telescope is the sensitivity which relates to its signal-to-noise ratio (SNR) available for observation [2]. The sensitivity is commonly expressed in system equivalent flux density (SEFD) according to

$$\text{SEFD} = \frac{2k_{\text{B}}T_{\text{sys}}}{A_{\text{eff}}}, \tag{2.7}$$

where A_{eff} is effective reflector area, T_{sys} the total system noise temperature and k_{B} the Boltzmann constant (in m^{2}Jy/K). If S_ν is the source flux density the SNR is calculated as

$$\text{SNR} = \frac{S_\nu}{\text{SEFD}}\sqrt{t\Delta\nu}, \tag{2.8}$$

where t is the integration time and $\Delta\nu$ is the available bandwidth. Therefore, minimizing SEFD results in higher SNR (lower RMS fluctuation) and shorter integration time needed

for detection. An increased available bandwidth, $\Delta\nu$, in the receiver also increases the SNR and reduces integration time. The sensitivity is sometimes expressed in $A_{\text{eff}}/T_{\text{sys}}$ with units of m^2/K which is just another form of (2.7) as $A_{\text{eff}}/T_{\text{sys}} = (2k_{\text{B}}/\text{SEFD})$. In the SKA project, this is the preferred notation to simplify for proportional expressions of array sensitivity. Both of these expressions include the effective area as a factor which means that a larger reflector would give higher sensitivity. Sometimes the sensitivity of different receiver systems are compared with the ratio $T_{\text{sys}}/\eta_{\text{a}}$ where the reflector area is not included.

2.4 System noise temperature

The total noise in a receiver system is represented by a system noise temperature, T_{sys}. For a single-pixel receiver the system noise temperature can be calculated according to

$$T_{\text{sys}} = \eta_{\text{rad}} T_{\text{a}} + (1 - \eta_{\text{rad}}) T_{\text{phy}} + T_{\text{rec}}, \tag{2.9}$$

where η_{rad} is the antenna radiation efficiency, T_{a} is the antenna noise temperature, T_{phy} the physical antenna temperature, and T_{rec} the receiver noise temperature. The latter includes the noise contributions from the receiver components such as possible bandpass-filters, couplers for calibration, and the LNAs, as illustrated in Fig. 2.2. Possible mismatches are also included in the receiver noise temperature. The antenna noise temperature T_{a}, represents the noise contribution to the system temperature from brightness sources surrounding the reflector system. In Section 2.5 contributions to T_{a} will be discussed together with the calculation model to estimate it.

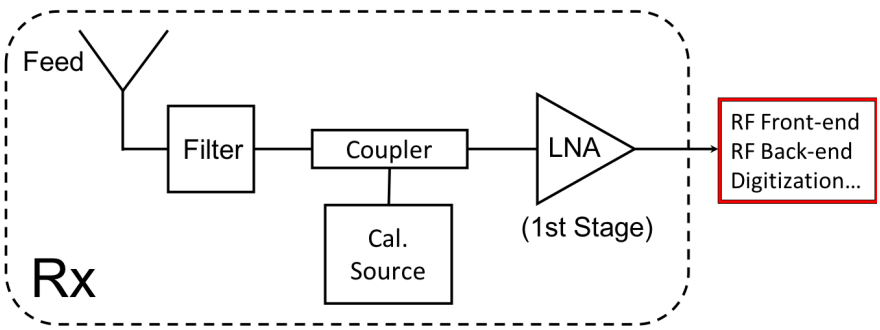

Fig. 2.2: Typical receiver chain illustrated.

2.5 Antenna noise temperature

In Fig. 2.3, $G(\hat{\boldsymbol{r}}, \theta, \phi, \nu)$ represents the beam pattern of the telescope which is pointing in the $\hat{\boldsymbol{r}}$ direction for observation, θ is the angle from zenith, ϕ azimuth and ν the frequency. The model of the surrounding brightness temperature, $T_{\text{b}}(\theta, \phi, \nu)$, seen by the telescope has several contributions [33]. These are mainly: emission caused by particles in our

atmosphere; sky brightness temperature seen as a background from space; emission from the ground, as well as scattering. $T_\mathrm{b}(\theta, \phi, \nu)$ therefore consists of one model for above the horizon, and one model for below the horizon

$$T_\mathrm{b}(\theta, \phi, \nu) = \begin{cases} T_\mathrm{sky}(\theta, \phi, \nu) & 0^\circ \leq \theta < 90^\circ \\ T_\mathrm{gnd}(\theta, \phi, \nu) & 90^\circ \leq \theta \leq 180^\circ \end{cases}, \tag{2.10}$$

with dependence of θ but assumed symmetric in ϕ. Therefore, the pointing direction of a telescope is generally denoted only with an angle in degrees given from *zenith*. In this thesis the zenith angle is denoted as θ_p, with zenith being $\theta_\mathrm{p} = 0^\circ$. Another way of giving the pointing direction (or sometimes tipping angle) can be as relative to the horizon in the form of elevation $\theta_\mathrm{elev} = 90 - \theta_\mathrm{p}$. It is unfortunately common to also use the notation θ for elevation which easily is confused with the spherical coordinate.

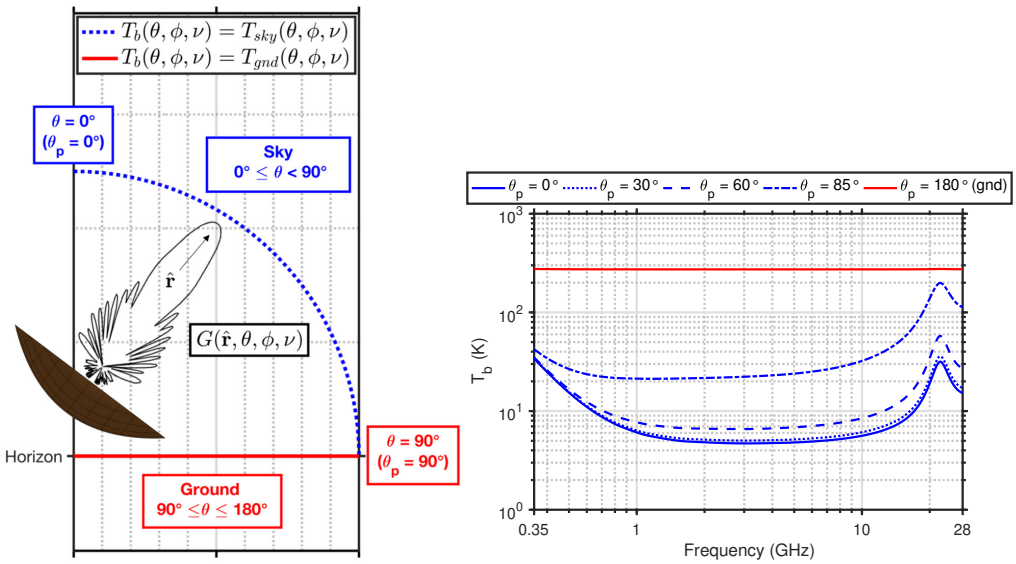

(a) (b)

Fig. 2.3: The concept of surrounding brightness temperature for a telescope is illustrated in (a). In (b) the brightness temperature, T_b, over 0.35–28 GHz for the SKA general model [33] is presented for some zenith angles. θ_p=180° represents T_b from the ground under the telescope.

The total antenna noise temperature, $T_\mathrm{a}(\hat{\boldsymbol{r}}, \nu)$, is calculated for each direction, $\hat{\boldsymbol{r}}$, and frequency, ν, through integration. The surrounding brightness temperature is weighted with the beam pattern of the telescope pointing in the direction of $\hat{\boldsymbol{r}}$ and integrated over the full-sphere

$$T_\mathrm{a}(\hat{\boldsymbol{r}}, \nu) = \frac{\int\int_{4\pi} G(\hat{\boldsymbol{r}}, \theta, \phi, \nu) T_\mathrm{b}(\theta, \phi, \nu) \, \sin\theta \, \mathrm{d}\theta \, \mathrm{d}\phi}{\int\int_{4\pi} G(\theta, \phi, \nu) \, \sin\theta \, \mathrm{d}\theta \, \mathrm{d}\phi}. \tag{2.11}$$

One major component in T_a is the inevitable background noise picked up from T_{sky}

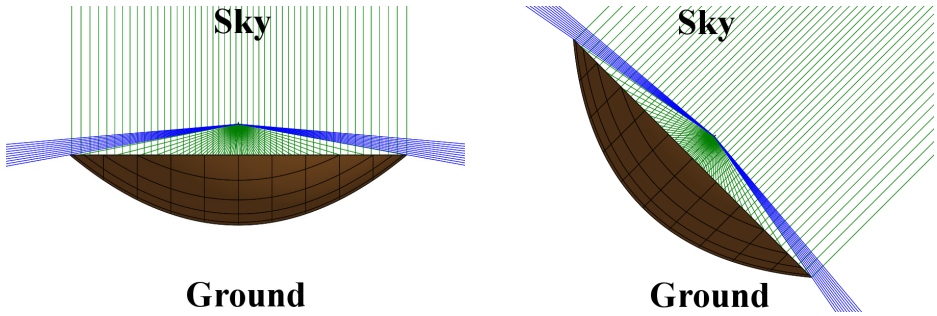

Fig. 2.4: Illustration of feed spill-over (blue) for an axisymmetric prime-focus reflector, dependent of pointing direction.

by the main-beam. Another important component to T_a is the noise picked up from spill-over power received from the ground. Both of these components are dependent on the zenith angle of the telescope. As the main-beam is pointing closer to the horizon (larger θ_p), the path through the atmospheric layer is longer, which increases T_a. In Fig. 2.4 spill-over is illustrated as the blue lines for a prime-focus reflector. The noise temperature contribution from spill-over depends on how much of it is terminated on the ground compared to on the sky. This can change significantly with θ_p depending on the feed design and reflector geometry. With an approximation of (2.11), the antenna noise temperature can be calculated by a simple equation using η_{sp} [28]. The antenna noise temperature is then given according to

$$T_a = \eta_{sp} T_{sky} + (1 - \eta_{sp}) T_{gnd}, \tag{2.12}$$

where $\eta_{sp} T_{sky}$ is the noise picked within the specified θ_e and can be assumed to be terminated mostly on the sky. This would be the main-beam contribution T_{mb}. The term $(1 - \eta_{sp}) T_{gnd}$ represents the spill-over noise temperature, T_{sp}, which is picked up from outside the subtended angle. For an axisymmetric prime-focus reflector (Fig. 2.4), the feed is pointing toward the ground (symmetric spill-over only for zenith), and this approximation could be argued as reasonable. This of course depends on possible back-lobe and side-lobe levels, diffraction and scattering. For a dual-reflector system such as the offset Gregorian reflector, particularly spill-over contributions are not as straightforward. In Fig. 2.5 the spill-over from feed towards sub-reflector (blue) and sub-reflector towards main-reflector (red) are illustrated. Due to the asymmetry of the structure, the spill-over contribution is also dependent on which direction the telescope is tipping [13]. When the feed moves away from the ground to point the telescope closer to the horizon, it is defined as *feed-up* configuration seen in Fig. 2.5b. If the feed moves towards the ground to point the telescope closer to the horizon, it is defined as *feed-down* configuration seen in Fig. 2.5c. By using a spill-over shield for the feed-down configuration, spill-over can be reduced significantly [13], [34]. Due to the asymmetry of the reflector geometry, the spill-over dependence on zenith angle, can also vary between the two orthogonal polarizations. To account for all the effects of such a complex geometry, the full calculation of (2.11) will

give a more representative result than (2.12).

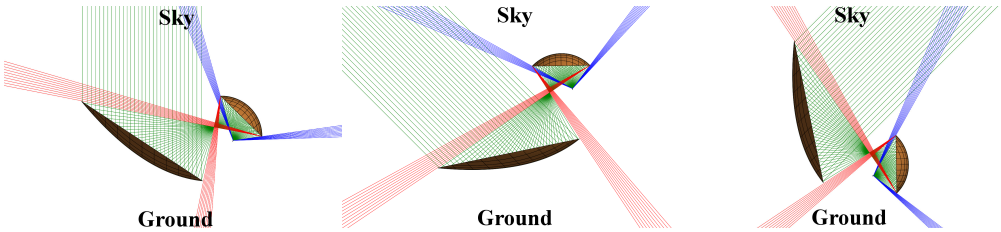

(a) (b) (c)

Fig. 2.5: Illustration of feed (blue) and sub-reflector (red) spill-over dependence on tipping direction for an offset Gregorian reflector. (a) Zenith; (b) Feed-up configuration; (c) Feed-down configuration.

2.6 Intrinsic cross-polarization

For radio observations, there is a desire to study the polarization state of sources. This requires the telescope, with receiver system, to be able to measure the orthogonal polarization components, i.e. it must be dual-polarized. Systems that can do this separation are generally called polarimeters. Typically, cross-polarization ratios are used as the FoM for polarimeters. The intrinsic cross-polarization ratio (IXR) introduced in [35], is the only such ratio that is independent of the coordinate system. It can be understood as a measure of the relative error in a polarimeter. The IXR of a reflector telescope is calculated by extracting the maximum and minimum amplitude gain as the invariants of the reflector beam pattern's Jones-matrix. The Jones-matrix is formed from the two sets of orthogonal components, one set for each polarization, in the reflector beam patterns. Each row is formed from the response of one polarization. The two polarizations are denoted as vertical (V) and horizontal (H) corresponding to the telescope's axes of movement. The Jones-matrix is formed as

$$\mathbf{J} = \begin{pmatrix} \mathbf{G}_{\mathrm{VV}} & \mathbf{G}_{\mathrm{VH}} \\ \mathbf{G}_{\mathrm{HV}} & \mathbf{G}_{\mathrm{HH}} \end{pmatrix}, \tag{2.13}$$

where $\mathbf{G}_{\mathrm{XX}}$ is the reflector beam pattern corresponding to each polarization's orthogonal components (i.e. co- and cross-polarization). From a single-value decomposition of (2.13), the maximum and minimum amplitude gain, denoted as $g_{\max}$ and $g_{\min}$ respectively, can be extracted. IXR is calculated according to

$$\mathrm{IXR} = \left(\frac{g_{\max} + g_{\min}}{g_{\max} - g_{\min}} \right)^2, \tag{2.14}$$

where a large IXR indicates that $g_{\max}$ and $g_{\min}$ are close in value, resulting in a better polarimetric response. For the SKA-MID feed systems on the SKA reflector, the IXR is

required to be better (more) than 15 dB within half-power beamwidth (HPBW) over the specified frequency bands.

CHAPTER 3

Ultra-wideband Feed Design - Quad-Ridge Flared Horn

The sensitivity for observations with a reflector telescope system depends on several factors. The larger the receiving area is, the more incoming radio energy can be collected. How efficiently this is done is one key to a sensitive system. Another very important factor is that the receiver itself must be designed as a low-noise, well calibrated, electronics system which is headed by the feed antenna. How optimal the feed converts the incoming radio waves into electric signals is crucial. For wideband and ultra-wideband feeds, high sensitivity over the large bandwidth is a challenge, especially due to inconsistent illumination from the feed's beam pattern over frequency. This leads to possible under- or over-illumination of the reflector, with potential spill-over noise degrading the system performance. Typically the impedance match is difficult for very wide bandwidths. The receiving SNR for detection will increase proportional to the square root of available bandwidth and integration time. A single wideband feed system can also cover a frequency range that otherwise requires multiple narrowband systems. Generally, a limited space is available in each telescope for the receiver systems and each of these systems are cryogenically cooled, which require moving parts. For a set of several hundreds of telescopes, as in the case of a large interferometric array, multiple narrowband systems increase the cost and maintenance time substantially. The complexity allowed for the telescope architecture, with an increasing number of receiving systems, eventually limits this approach. By using a sensitivite wideband system instead, costs for manufacturing and maintenance can be reduced. It can also reduce power consumption and the available space needed to house the receiver. Highly optimized wideband feeds and receiver systems are therefore very attractive. An impressive amount of work during the last two decades has been put in to development of different kinds of UWB feeds for radio telescopes. Examples are the: Antonio Feed [12]; Eleven-Feed [19], [20]; Quasi-Self-Complementary Feed (QSC) [21] and the Quad-ridge Flared Horn (QRFH) [22], [23], [24], [25]. In this chapter the focus is on wideband and UWB design of QRFHs as reflector feeds for radio telescopes. The text serves as an overview of current state-of-the-art QRFH performance, typical design processes and techniques together with the new development introduced in the papers of this thesis.

3.1 Ridge waveguide

The ridge waveguide technology was initially realized by loading regular waveguides with a dual-ridge structure [36], [37]. The dual-ridge structure increases the bandwidth (single-mode) as it lowers the cut-off frequency by a factor of four compared to a same-sized regular waveguide. The quad-ridge waveguide [38] actually has less (single-mode) bandwidth than the dual-ridge, due to mode splitting that also reduces the cut-off for higher order modes. Despite this, quad-ridge structures are still interesting as many applications do not require single-mode bandwidth. The quad-ridge structure also enables dual-linear polarization which is desired in many applications, e.g. space geodesy and radio astronomy.

3.2 Quad-ridge flared horn

The quad-ridge flared horn (QRFH) is a flared-out section of a quad-ridge waveguide made from low-loss metal with a sturdy structure, illustrated in Fig. 3.1a. Because of the quad-ridge structure, it provides dual-linear polarization without the need for an orthomode transducer (OMT). QRFHs are normally designed for single-ended excitation which only requires one LNA per polarization, and thus keeps the complexity low. To excite the two orthogonal polarizations, coaxial-type launch-pins can be used. For each set of ridges, the launch-pin is fed through one ridge and contacted on the opposite ridge, as shown in Fig. 3.1b. An optimized QRFH design can generally achieve input reflection coefficient less than -10 dB for 6:1 bandwidth [22]. This results in a very compact design, especially for deep reflector configurations, which is straightforward to integrate together with LNAs in a cryostat dewar for low-noise applications, see Fig. 3.1d. The excication point of single-ended QRFHs is clearly asymmetric due to the offset in boresight between the launch-pin, as seen in Fig. 3.1b. The result is slightly different input reflection coefficients for the two polarizations. This can be compensated for, by removing a distance equal to the offset from the back-short cut of the ridges to the bottom horn, for the polarization excited further up. It has been shown that quadraxial feeding can be used for the QRFH with the benefit of high-order mode suppression [23]. However this approach complicates the receiver integration and requires either differential LNAs, which are more expensive, or a hybrid setup with four single-ended LNAs. QRFHs have been designed as reflector feeds with f/D between 0.3 to 2.5 [39] using both square and circular waveguide structure for UWB bandwidth [40]. Most QRFH designs for radio telescopes, use circular waveguide structure and the intended reflector geometry typically has $0.35 < f/D < 0.5$. The waveguide properties of QRFHs give a sharp lower cut-off frequency which mitigates radio frequency interference (RFI). The shape and structure is usually straightforward to manufacture with simple and low-cost methods for assembly. Because of the bandwidth, compact design, robustness and single-ended feeding, the QRFH is a popular choice as an UWB feed. It is also scalable in frequency in a straightforward way. The radio astronomy community is always looking to expand the observational bandwidths in frequency. The LNAs of today can achieve excellent low-noise performance over decade bandwidth [15], [17]. The digitzer and back-end technology is

progressing fast towards larger bandwidth [26]. Therefore, there is a need for UWB feeds to match these components in operational bandwidth. The QRFH technology has many benefits compared to other UWB feeds, but also some remaining challenges. To compare with high-sensitivity narrow-band feeds, the QRFH design for wideband frequency ranges, should be developed further. For UWB bandwidth, the QRFH suffers from a narrowing beamwidth especially in H-plane. To address these issues without jeopardizing the simple concept of the QRFH, is therefore a valuable approach. With this in mind, and practical aspects of designing a feed for integration in a radio telescope receiver, the work in this thesis adds to the QRFH knowledge reserve.

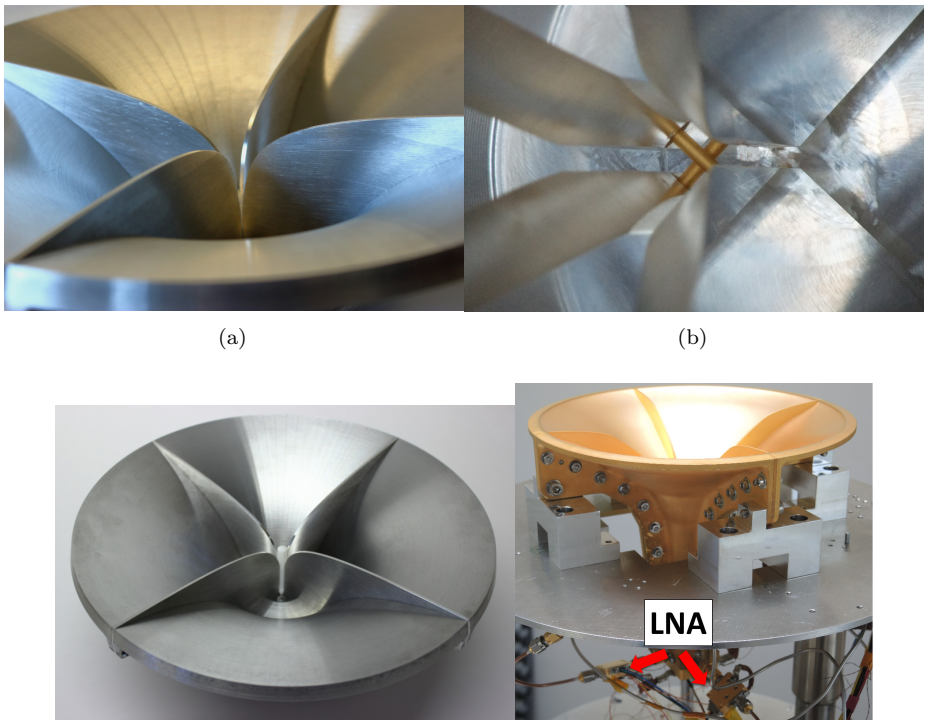

(a) (b)

(c) (d)

Fig. 3.1: (a) Flared-out ridges; (b) Typical crossing launch-pins for single-ended feeding; (c) QRFH loaded with a dielectric cylinder for decade bandwidth. (d) QRFH integrated in a test dewar together with LNAs for cryogenic tests.

3.2.1 Profile shape

The shape of the QRFH is constructed from two profiles, one for the horn shape and one for the inner shape of the ridges, as illustrated in Fig. 3.2a. The flared-out shapes of the QRFH horn and ridges are typically modeled by analytic expressions such as: exponential, sinusoidal, tangential [22], [23]. This approach has proven to give good performance over

multi-octave bandwidths, with relatively few parameters to include in the optimization. A typical profile, defined separately for the horn and ridge, is the exponential expression

$$x(z) = A\left(\frac{r_\mathrm{a} - r_\mathrm{t}}{e^{RL}-1}e^{Rz} + \frac{r_\mathrm{t}e^{RL} - r_\mathrm{a}}{e^{RL}-1}\right) + (1-A)\left(r_\mathrm{t} + (r_\mathrm{a} - r_\mathrm{t})\frac{z}{L}\right), \tag{3.1}$$

where r_t and r_a are the throat and aperture radius, respectively. L is the taper length, R is the exponential opening rate, and A is the linear taper in each profile [22]. For more degrees of freedom, a spline-defined profile could be used, as was shown in Paper A, Paper B and [41]. The spline-defined profile is constructed from a number of points which each has a "x" (width) and "z" (height) coordinate. The points are splined together for a full profile. In Fig. 3.2b the difference between an exponential and spline-defined profile is illustrated. The approach of analytic expressions typically generates a constantly increasing radial flare of the QRFH. With a spline-defined shape, the profile has more degrees of freedom that can result in a more custom shape. The Band 1 QRFH design did, during early optimization, suffer from a sharp resonant mode phenomena at two frequency points in the band. This form of "trapped mode" was removed when the splined horn profile was optimized into the hour-glass shape, initially presented in Fig. 4 of [42] and further improved in Paper B. The hour-glass shape could be understood as implementing a form of higher-order-mode suppression, previously implemented as a ring in the bottom of QRFHs [43]. The drawback of the spline-defined profile is a significant increase to the parameter search space for optimization.

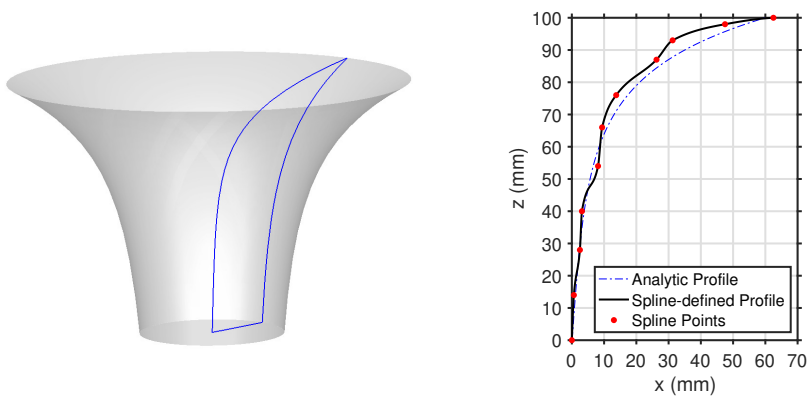

(a) (b)

Fig. 3.2: (a) QRFH shape from profiles; (b) Exponential and spline-defined profile;

Analytic-Spline-Hybrid profile

Another approach is to use a combination of the analytic and spline-defined profiles. With this approach, the horn shape can be divided in sections which are either defined

through analytic expressions or splines, as illustrated in Fig. 3.3. A two-step optimization schematic of an Analytic-Spline-Hybrid (ASH) profile resulting in a slightly improved aperture efficiency compared to an analytic profile, was introduced in Section V of Paper C . Potentially this could offer further control of the QRFH impedance match, beamwidth and higher order mode-suppression. In [41] the complete spline-defined profile was successfully optimized for different sections of the horn separetely before optimizing it all together. One drawback of the ASH approach is the increased complexity of the optimziation scheme. However, partly defining the profile with an analytic expression would reduce the number of parameters (time) in optimization compared to a purely spline-defined profile. So far only small improvements have been shown with the ASH approach (Fig. 8 of Paper C) for specific scenarios, and further investigation is needed.

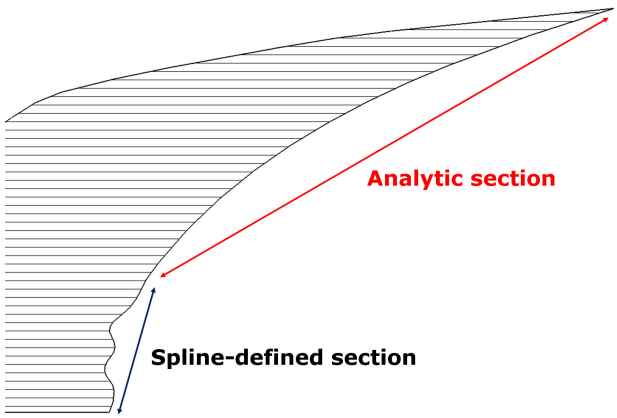

Fig. 3.3: Analytic-Spline-Hybrid profile illustrated for the QRFH.

3.2.2 Design optimization

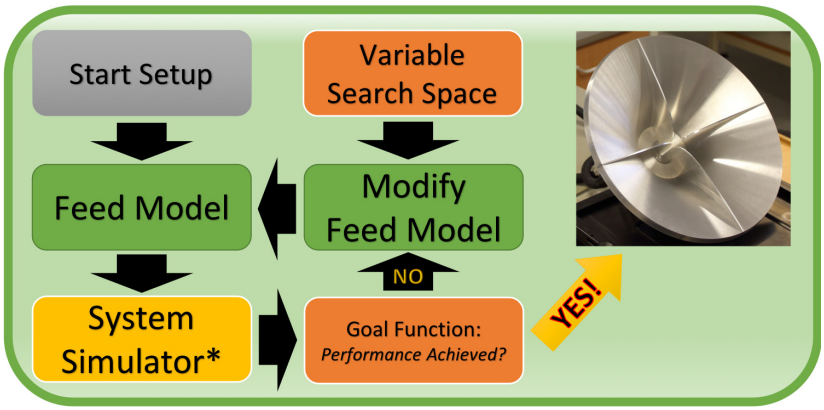

Fig. 3.4: Typical optimization scheme in wideband feed design. *System simulator can be different depending on the application.

Typically QRFH feeds (and UWBs in general) are designed with numerical optimization of a parameterized model. In Fig. 3.4, a common approach for UWB feed optimization for a reflector geometry is illustrated. For this type of complex, large search space a stochastic optimization algorithm scheme is used to control the process, e.g. particle swarm optimization (PSO) [44]. PSO can search large variable spaces and does not need a gradient to direct the optimization forward. Commercially available EM simulators and toolboxes have internal optimization frameworks available that include a choice for stochastic algorithm. The approach to use MATLAB to control CST MWS and TICRA's GRASP in a scripted loop can give a full beam pattern evaluation of each iteration relatively fast. The choice of QRFH profile influences how many parameters are included in the optimization. QRFH based on analytic profiles typically have 15–20 parameters [24] and spline-defined profiles have been designed with up to 60 parameters [41]. Other parameters not defined by the profiles are: ridge thickness; separation between opposing ridges; separation between adjacent orthogonal ridges; size and shape of the back-short structure to compensate for the asymmetric excitation; excitation point location in height. The starting point for the waveguide structure can be chosen from analytic calculations of the dominant mode's (circular: TE_{11}) low-frequency cut-off [38]. Due to the large number of designed QRFH feeds available in research, generally good starting dimensions can be found in the literature for the most common frequency bands. Ideally, optimization is set up with a goal function that finds the global minimum without additional input. However, this brute-force approach to optimizing a UWB feed over many frequency points is relatively time-consuming. Therefore, multiple optimization runs are usually required to reach the desired specifications, with modifications in between runs. Typically, when a model close to the desired specification is achieved, a local optimization algorithm can be used for fine-tuning. Interesting performance characteristics specified in the goal function are input reflection coefficient and port isolation, sensitivity, aperture efficiency, and

cross-polarization. Depending on the application, feed size and weight can be important limiting factors that need to be included as well. In an offset Gregorian reflector for example, the feed/receiver can physically block the incoming waves if it is too large. A pitfall in the optimization could be, to use too strong weighting on specific goals that steer the algorithm towards a local minimum early in the process which limits the final performance. For example, weighting the goals for $A_{\text{eff}}/T_{\text{sys}}$ and η_{a} equally, can result in less than optimal $A_{\text{eff}}/T_{\text{sys}}$, even though A_{eff} is proportional to η_{a}. $A_{\text{eff}}/T_{\text{sys}}$ is also dependent on the surrounding parameters as receiver noise, reflector geometry (spill-over shield, available area), and the surrounding brightness temperature at the frequencies of interest. Finding an optimal goal function in reality includes trial-and-error for the specific setup. Therefore, the need is evident for an accurate and fast system simulator in feed design, especially for a complex FoM based on several input variables - which is the case for sensitivity.

3.2.3 System simulator

To achieve a highly optimized reflector-feed-system, the full system performance needs to be predicted with good enough accuracy and speed during the design phase. For UWB feeds the frequency resolution used must be fine enough to represent the large bandwidth. This is because UWB performance can be rapidly fluctuating over the bandwidth, with sharp resonances not visible if the frequency step is too coarse. For optimization with many thousands of iterations, the system simulation must therefore be accurate and fast for realistic design time. Today there are many powerful EM-simulator software packages (e.g CST MWS, FEKO, TICRA GRASP, HFSS) that offer a variety of toolboxes for this purpose. For a high sensitivity optimization, each model iteration must be evaluated on the specified reflector with spill-over, gain and cross-polarization simulations. For the wideband feed presented in Paper A and Paper B the system prediction was performed with a dedicated simulator [45]. In Fig. 3.5a, the schematic of an iteration for that MATLAB/CST/GRASP-based simulator is illustrated with the main steps. The CST feed pattern is imported to the reflector model in GRASP. The reflector beam patterns in GRASP are calculated with physical optics (PO) and physical theory of diffraction (PTD). From these patterns, the effective area A_{eff} and the IXR are calculated (among other things). The reflector beam patterns are also used to weight the provided brightness temperature model [33] for antenna noise temperature calculation according to (2.11) over all frequencies and zenith angles. Sensitivity is calculated from A_{eff} and T_{sys} according to (2.7) and (2.9). This method has been proven to be accurate compared to full-wave simulations [46]. For low frequencies, the fullsphere PO+PTD simulation of a 15 m dish is quite fast with only a few minutes for maximum frequency. The integration mesh needed is relatively coarse, and therefore suitable for a large number of iteration. For high frequency feeds (without significant back-lobes), the system simulation can be done by approximate methods where the main-reflector is masked to reduce calculation time significantly [47],[48].

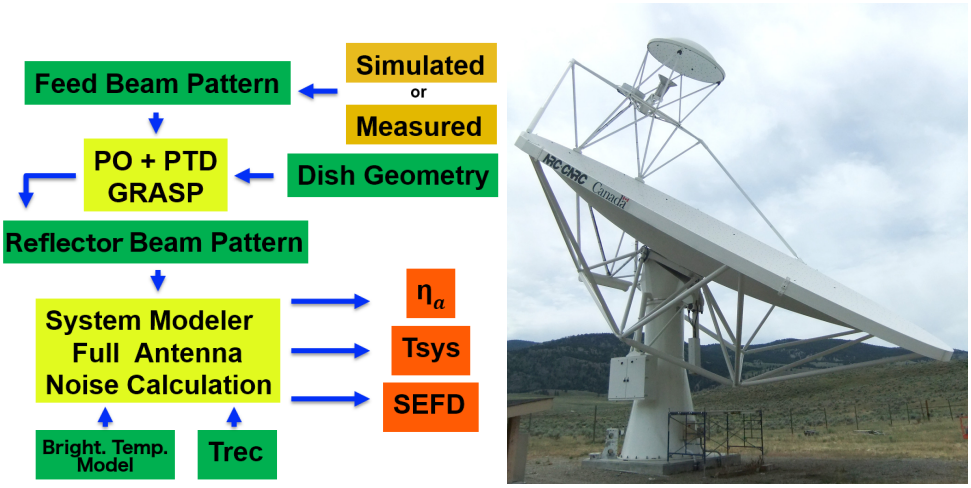

(a) (b)

Fig. 3.5: (a) Schematic of the PO+PTD system simulator that models the feed performance on a reflector system; (b) Example of a complete reflector system that can be modeled with the system simulator. The image shows the first SKA Band 1 QRFH prototype mounted on the Dish Verification Antenna 1 (DVA1) in Penticton, BC, Canada in 2016.

3.2.4 Beam pattern measurements

Measured feed beam patterns can be characterized conveniently for most QRFHs with frequencies larger than 1 GHz in either a nearfield or farfield anechoic (non-echo) chamber, as shown in Fig. 3.7. The farfield region starts at a distance of $2D_L^2/\lambda$, where D_L is the largest linear dimension of the antenna. The nearfield chamber use a Fourier transformation to turn the measured nearfield into the farfield. Standard gain-calibration is performed using standard gain horns under specified accuracy [49]. QRFHs for frequencies below 1 GHz are large and heavy structures which could be difficult to mount in an anechoic chamber. For the SKA Band 1 frequencies 350–1050 MHz for example, the wavelengths are up to 0.85 m for the QRFH. The horn size is therefore in the order of 1 meter both in height and diameter which makes the horn difficult to handle in a small chamber. The first confirmation of beam pattern performance was therefore performed indirectly with reflector beam pattern measurements, as presented in Fig. 3 of Paper A. The feed is mounted on the reflector dish, as illustrated in Fig. 3.5b, and the telescope main-beam is swept across a bright source. It is important to apply appropriate corrections for efficiency, elevation deformation and source solid angle [27]. Since the end-goal of the feed is to illuminate the reflector, this is the more interesting beam pattern measurement. It does however, result in a much more demanding setup. Furthermore, it does not provide specific information on feed or reflector far-out side-lobe levels. To be able to predict the full reflector beam pattern in the whole 4π sphere for a large reflector, accurate simulations are needed. To be able to measure the same reflector beam pattern response

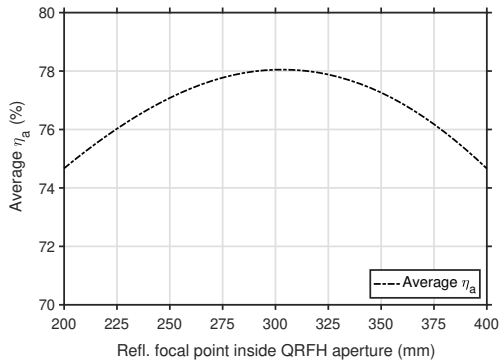

Fig. 3.6: Illustration of change in aperture efficiency, η_a, depending on the feed's location relative to the reflector focal point on the optical axis.

that was simulated, it is important that the feed's location relative to the reflector focal point is consistent. This is because of the feed location-dependence in the phase efficiency, η_{ph}, when illuminating the reflector. Aperture efficiency, η_a, can vary significantly over the band depending on η_{ph} (2.4). In Fig. 3.6 an illustration of how aperture efficiency for a low-frequency QRFH (< 1 GHz) changes when the feed location is varied over a range of 200 mm relative the reflector focal point on the optical axis. For a feed of higher frequency and large bandwidth, this variation can be more severe and large deviations can be caused by misplacement of only millimeters. To practically realize the correct feed location on the reflector, a good reference point for the mechanical mounting should be provided. This can be done by first optimizing the location in simulations, to achieve maximum phase efficiency in the upper range of the frequency band as it is more sensitive to spatial variation [50]. Then, a simple reference point for mechanical installation can be calculated using the QRFH aperture as reference. Typically for optimal performance, the reflector focal point should be located some distance inside the horn, measured from the QRFH aperture. In most EM simulators the feed beam patterns can be exported with coordinates relative to the aperture for consistent calculations of reference location in the reflector. This reference point is also important during optimization, so that the location of the feed does not block the ray-path of the reflector. This was the case for the SKA Band 1 feed, due to the large size of the feed. Therefore, constraints were set in the optimization on the feed size and the feed reference location.

3.2.5 Receiver noise temperature measurements

During optimization the receiver noise is modelled with an estimation from LNA noise-data and expected noise contributions from other receiver components. The feed losses are also included. For a realized system, the receiver noise temperature should be measured and one could implement different techniques. The hot-cold Y-factor measurement is a well established approach [51] and can be implemented without installing the feed on the reflector. In Y-factor tests, the power at the output of the receiver is measured

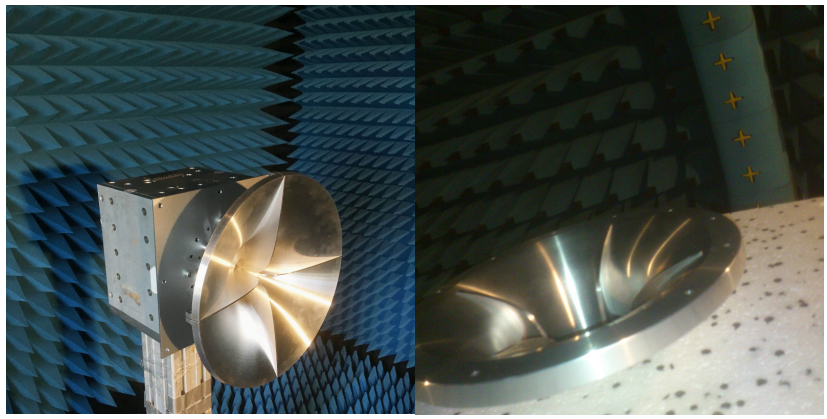

(a) (b)

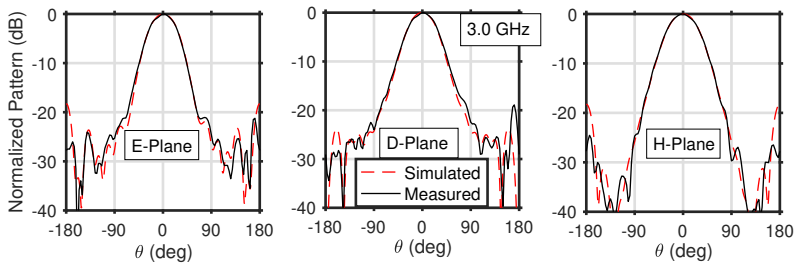

(c)

Fig. 3.7: (a) QRFH in anechoic farfield chamber where the feed sweeps in azimuth; (b) QRFH in anechoic nearfield chamber with the arc containing the dual-polarized transmitting antennas; (c) Measured co-polarization beam patterns in E- (ϕ=0°), D-(ϕ=45°), and H-(ϕ=90°) plane at 3 GHz for a QRFH covering 1.5–4.5 GHz.

in two steps. The first step is when the antenna main-beam is terminated in a known hot load and the second step is when it is terminated in a known cold load. The linear Y-factor is then given by the power ratio $P_{\text{hot}}/P_{\text{cold}}$ off the two measurements. The Band 1 receiver noise was measured in the hot-cold test facility (HCTF) at DRAO, Penticton in Canada. The HCTF is a large flared-out metal box with a sliding roof which is padded with absorbers on the inside, Fig. 3.8. The layout prevents possible back- and side-lobes from the feed to hit the ground and instead terminates them (most likely) on the sky. In this case the hot load is the absorbers' physical temperature T_{hot} and the cold load temperature T_{cold} is the sky background brightness. The beam-pattern of a relatively low-gain QRFH covers a broad solid angle, so T_{cold} should be calculated according to (2.11). In this case $G(\theta, \phi, \nu)$ is the beam-pattern of the feed pointing to zenith, simulated

inside the HCTF. T_{rec} is calculated from the Y-factor according to

$$T_{rec} = \frac{T_{\mathrm{hot}} - YT_{\mathrm{cold}}}{Y - 1}. \tag{3.2}$$

In Fig. 2 of Paper A, good agreement is found between estimated and measured receiver noise for SKA Band 1 using Y-factor tests. The agreement is presented by using both data sets to calculate the sensitivity. The typical error in the Y-factor technique should be in the order of a few percent. It is important to confirm T_{rec} with measurement to find any severe mismatches between the manufactured feed, couplers and LNAs, or unexpected resonant behavior in the receiver chain.

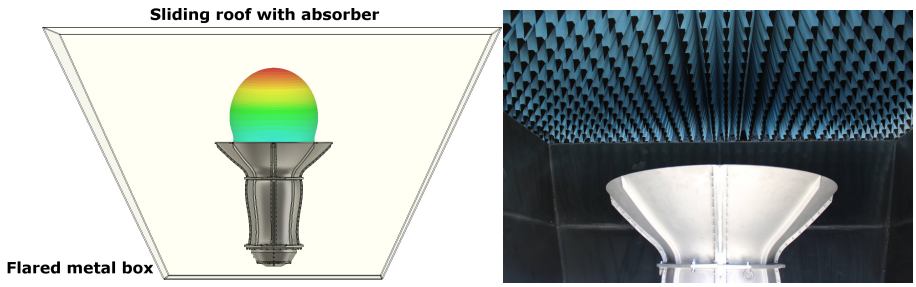

(a) (b)

Fig. 3.8: (a) Concept of the hot-cold-test-facility (HCTF); (b) QRFH in the HCTF.

3.3 Room temperature system

For QRFHs below 1 GHz, or designs for shallow reflector configurations, the large size of the horn makes integration inside a dewar extremely difficult. The feed can no longer be completely cryo-cooled. Instead a thermal break between the horn and dewar is needed [42], assuming the LNAs are cryogenic. The connecting cables must be long enough to reduce the thermal gradient and not keep cooling power low. The thermal break introduces a noise contribution before the LNA. The trade-off between noise and thermal load must be optimized. Ideally, the LNAs would connect directly to the launch-pin of the QRFH. However, this would introduce a more complex vacuum break with cryogenic cooling of the lower part of the feed. This technique has been succesfully implemented by other types of feed systems [46]. Another approach is to use room temperature LNAs which today achieve very low noise temperature at these low frequencies [52]. If the ridges are thick enough, the LNAs can be integrated directly inside the metallic structure and connected to the launch-pin mitigating additional losses. This approach was succesfully implemented for the SKA Band 1 QRFH where the ridges were designed thick enough, so that they could be hollowed out at the excitation point for LNA integration, as shown in Fig. 1 of Paper B. The noise injection is built into the room temperature LNAs which were provided by Low Noise Factory (LNF), Gothenburg, Sweden. Compared to the previously proposed cryogenic design with a thermal break, the final receiver noise temperature is

similar (Figure 15 in [46]). The room temperature system has obvious advantages in reduced cost, complexity, and maintenance time. There is also no need for a cryostat which reduces power consumption.

3.4 Design for high sensitivity

Fig. 3.9: Final prototype of the SKA Band 1 QRFH. Image credit: Chalmers/Johan Bodell.

The figure-of-merit for radio telescope receiver systems, is ultimately the observational sensitivity. To achieve high sensitivity several factors should be taken into account. The reflector geometry and frequency band are important for the design. The total system noise temperature is important, but also the individual size of its components (2.9). The improvement done by reducing the spill-over a few kelvin, depedends on if the receiver noise and sky brightness are in the same order of magnitude. The effective area A_{eff} is clearly dependent on the reflector area, where a very large reflector has more to gain in improved aperture efficiency. The contribution to the system noise temperature from current state-of-the-art LNAs, can be as low as a few kelvin for cryogenic designs [16] and 8–10 K for room temperature designs [52], depending on bandwidth and frequency. The noise increases with frequency and with bandwidth as it is more difficult to impedance-match LNAs over large frequency bands. The LNA's noise contribution at frequencies below ∼20 GHz is comparable in size to the spill-over and sky brightness contributions. This puts stronger emphasis on reducing the spill-over noise for the reflector feed system. The feeds for SKA are optimized for high sensitivity, $max(A_{\text{eff}}/T_{\text{sys}})$, with a required absolute level that must be achieved over each frequency band. The SKA Band 1 feed package fulfills the sensitivity specification over $\theta_{\text{p}} \in [0°, 60°]$ required for the SKA, as shown in Fig. 4a of Paper B. It achieves high and stable aperture efficiency with an average of 80% and maximum of 85% over 3:1 bandwidth. As a way to reduce edge diffraction, the QRFH was designed with an aperture-matching shape [53]. For frequencies

below 600 MHz the galactic brightness temperature contribution is significant, as shown in Fig. 2.3. For 350 MHz, T_{sky} is in the order of 35 K, which is seven times the spill-over contribution ($\theta_{\mathrm{p}} = 60°$) and two times the receiver noise temperature at this frequency for SKA Band 1, see Fig. 3.10. This results in a lower achievable sensitivity than at the upper frequency range. At 900 MHz the contribution from the sky brightness is in the order of 7-8 K and spill-over close to 2 K, and therefore a higher sensitivity goal is realistic. The shaping of the offset Gregorian reflector has typically proven to

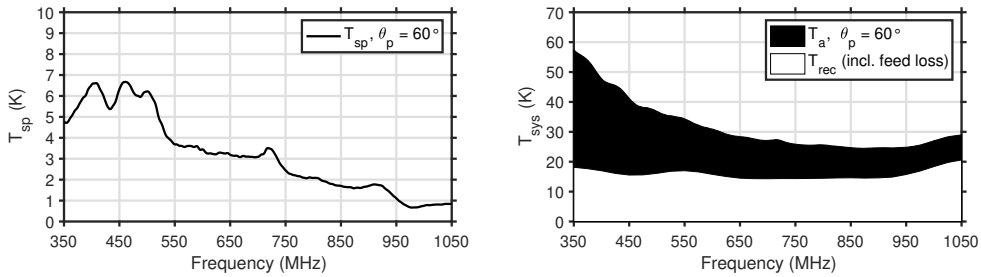

Fig. 3.10: (a) Spill-over noise, T_{sp}; (b) Total system noise, T_{sys} for the SKA Band 1 feed simulated on the SKA dish.

increase the systems aperture efficiency up to ∼10%. For the shaped 15 m SKA offset Gregorian, a spill-over shield is also implemented that extends 40 degrees downward from the sub-reflector [34]. In the feed-down configuration, the shield mitigates ground spill-over pick-up from the feed. The spill-over shield concept is illustrated by a generic offset Gregorian dish in Fig. 3.11. Compared to the non-shielded concept in Fig. 2.5, the spill-over shield improves the system sensitivity significantly (illustration in Figure 6 of [13]). The feed-down configuration also allows for installation and maintenance with the feeds in a horizontal position close to the ground. The optimal spill-over and aperture

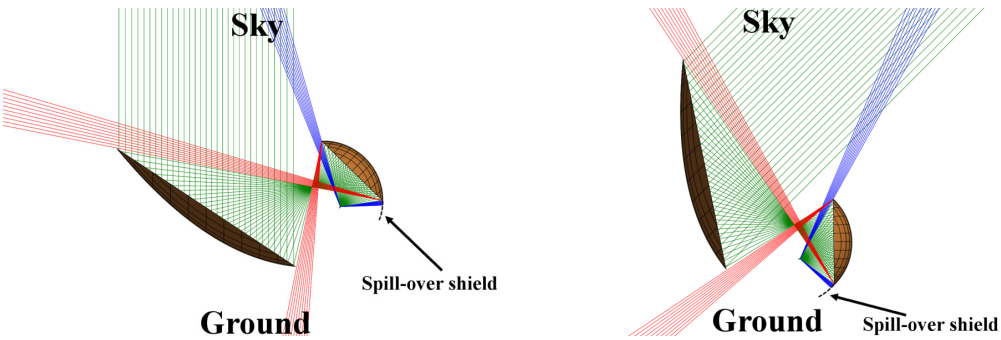

Fig. 3.11: Illustration of the spill-over shield effect.

efficiency achieved for a feed, are specific to the reflector geometry that the feed was designed for. The sensitivity is also proportional to the reflector diameter and hence the

performance of a certain feed package can therefore be very different between reflector geometries. For example, the SKA Band 1 is optimized for high sensitivity on the shaped SKA dish with an optimal edge-taper of -12 dB at $\theta_e = 58°$. The MeerKAT dish requires a similar edge-taper, but at a smaller $\theta_e = 49°$. This results in over-illumination of the MeerKAT sub-reflector from the SKA Band 1 feed and higher spill-over. Furthermore, the MeerKAT dish is unshaped with a smaller main-reflector diameter than the SKA dish, which results in a lower expected sensitivity when illuminated by the SKA Band 1 feed, see Fig. 3.12a. Both reflector configurations are feed-down. For high sensitivity on a specific reflector, UWB feeds should be tailored to that geometry. Once again this emphasizes the need for accurate and fast system simulation during optimization. In

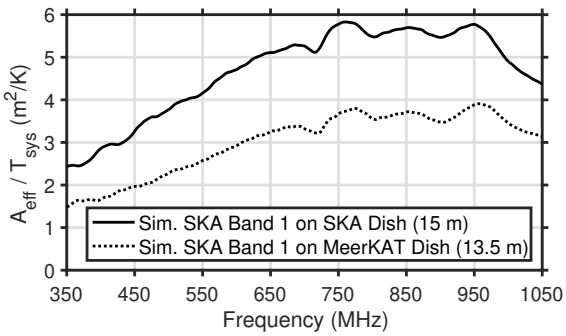

(a)

(b)

Fig. 3.12: (a) Sensitivity simulated of the SKA Band 1 feed package on 15 m SKA dish vs 13.5 m MeerKAT dish; (b) The SKA Band 1 feed package installed on a MeerKAT reflector for qualification tests.

Fig. 6 of Paper B, a good example of the obtained agreement between simulated and measured sensitivity is presented for the SKA Band 1 on a MeerKAT 13.5 m reflector. The PO+PTD system simulator (Fig. 3.5a) was used for the simulation. To measure the sensitivity, drift scans of known sources was performed. A general brightness model of the sky, such as [33] used here, does not account for the sky brightness near specific sources. Therefore corrections were applied in the results of Paper B by adjusting the brightness model. Another correction that was applied to the measured data, was for the slightly larger aperture available in the mechanical model of the reflector than in the theoretical simulation model. The tiles that make up the main reflector, extend the available surface of the mechanical model, as shown in Fig. 3.12b. For the MeerKAT reflector model, this difference in size is ∼7%. In the PO+PTD simulation, the mechanical structure that holds the sub- and main-reflector is not included, which also could affect the result. For example, back- and side-lobes from the feed could have a scattering effect at the indexer. However, the good agreement between simulation and measurement (Fig. 6 and Fig. 7 of Paper B), after the aforementioned corrections, indicate that the effect of the mechanical

structure is small. To predict all possible effects, a full-wave simulation of the mechanical reflector model, mounted with the feed, should be performed.

3.5 Dielectrically loading - for decade bandwidth

QRFH beamwidth consistency over a decade of frequency bandwidth is challenging. To also keep the QRFH structure simple is an important prerequisite to not jeopardize its practical benefits in receiver integration. Impedance matching has been performed succesfully above 10:1 bandwidth [54]. Despite this, the QRFH beamwidth decreases as the frequency increases over large bandwidths, especially in H-plane. High phase efficiency η_{ph} and low cross-polarization levels are also hard to achieve across 10:1 bandwidth. One approach to improve the beamwidth control, is to add dielectric material in some form into the QRFH structure [50], [55]. In [50], a three-layered dielectric load is designed together with the QRFH that also includes a choke-skirt attached to the aperture. The technique shows good results for the 6:1 bandwidth over 0.7–4.2 GHz with near-symmetric beam patterns in E-, D- and H-plane and low cross-polarization. The aperture efficiency is above ∼60% for $f/D = 0.41$ and input reflection coefficient less than -14 dB. However, the complexity of the QRFH design is increased in terms of optimization, manufacture, cost and assembly. For higher frequencies the dimensions would be smaller and a very complex structure can be hard to realize without expensive manufacture. To realize

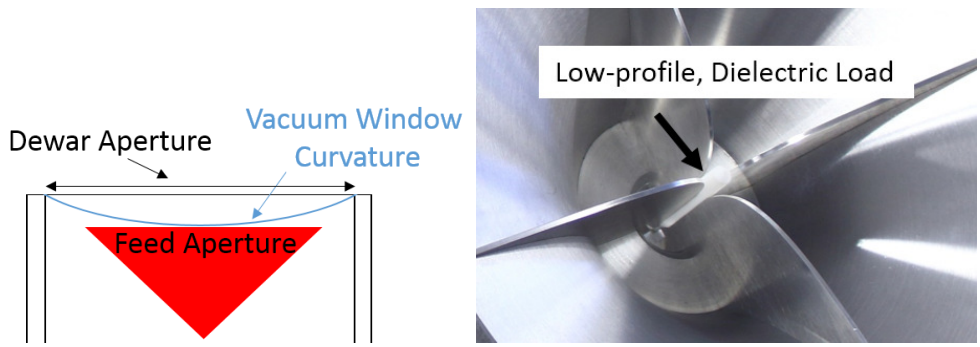

(a) (b)

Fig. 3.13: (a) Illustration of feed dewar integration; (b) Low-profile, cylinder-shaped, dielectric load installed in a QRFH.

decade bandwidth, a similar approach could be used but with an aim to also keep the QRFH simplicity intact. Unlike [50] and [55], the dielectric load proposed in Paper C and Paper D has a low-profile cylinder shape. It is installed in the center of the QRFH, towards the bottom, with plenty of clearance to the aperture, as shown in Fig. 3.13b. The proposed feed covers a decade frequency range of 1.5–15.5 GHz. The excitation is kept single-ended by feeding the launch-pins through a hole in the dielectric load. The low-

profile does not affect the footprint of the QRFH, keeping it compact and straightforward to integrate in a cryostat dewar. Generally, the feed needs to be placed with a certain spacing to the dewar aperture. This is due to the vacuum window's inward curvature from the pressure difference, illustrated in Fig. 3.13a. If the necessary clearance between the feed and the dewar aperture is too large, unwanted resonant affects or beam-splitting can occur. This was observed for a wide-beam QRFH prototype configuration when mounted too deep in a test dewar, as shown in Fig. 3.14. The beam-splitting effect shown here at the center of the band, is even more evident for the lower frequencies. This can drastically reduce the radiation properties and noise temperature performance of the model. The alternative to enlarge the dewar window would cause an unwanted increase in IR radiation that also would increase the power load significantly. For the ngVLA [11] and SKA [14], an important requirement is the power consumption of the compact receiver designs. Therefore, it is beneficial with a low-profile dielectric load to keep the QRFH footprint unchanged. This type of low-profile load made from a one-layered

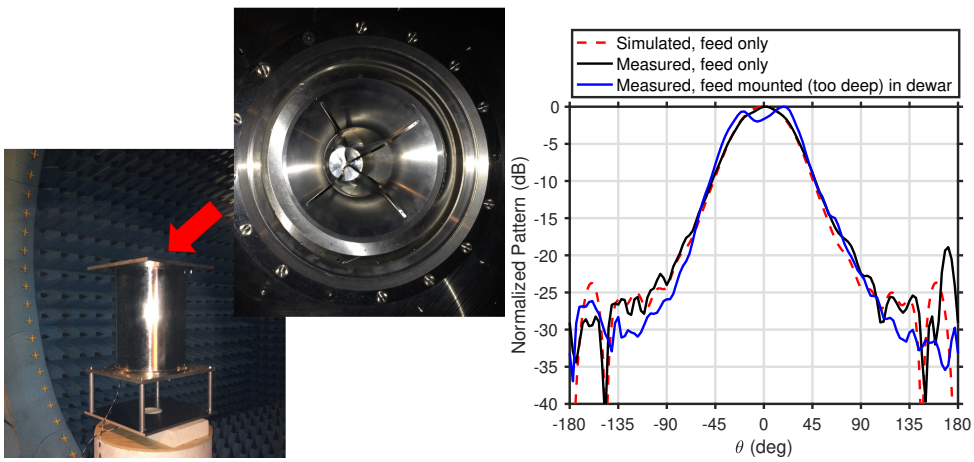

(a) (b)

Fig. 3.14: (a) Test dewar for a 3:1 QRFH feed, illustrated without vacuum window. (b) Measured beam pattern at center frequency, 3 GHz, show beam-splitting effect because the feed is mounted too deep in the dewar.

low-loss dielectric material (Polytetrafluoroethylene (PTFE, "Teflon") is machinable in one piece. This makes it attractive for large scale production in terms of cost and assembly. The losses due to the dielectric can typically be in the order of only a few kelvin for cryogenic temperatures, depending on frequency and material. Due to the small size and one-layered structure of the dielectric load, it mitigates the risk of non-homogeneous cooling throughout the material. By clamping the dielectric load between ridges and bottom lid of the QRFH, thermal contact is made. It also prevents it from sliding out or wobbling, when the telescope is in motion. The simplicity of the approach makes the idea feasible to use it to upgrade existing QRFHs. The shape of the dielectric could easily be

optimized for an existing QRFH design.

3.5.1 Wide beamwidth for deep reflectors

Most QRFHs being used in radio telscopes today, are designed for f/D ratios between 0.35 and 0.5. More work needs to be done for deeper reflectors, as pointed out on pp. 79 in [24]. In Fig. 3.15 the deep ($f/D = 0.3$) axisymmetric prime-focus reflector of the Effelsberg 100 m telescope is illustrated with a simplified model. The corresponding half-subtended angle is θ_e=79.6°, which is a challenging beamwidth to illuminate with an UWB feed. Typically this configuration would use a choke-type horn that can achieve wide beamwidth over narrow frequency ranges. For QRFHs, the spill-over efficiency tends to increase with frequency over the bandwidth as the beam gets narrower. The low frequency part of the band suffers the lowest spill-over efficiency, which for a prime-focus application is more severe as the feed is pointing towards the ground. For a large prime-focus reflector this can still be acceptable due to the large effective area enabled, if good aperture efficiency is achieved. For an extremely large reflector such as the Effelsberg 100 m dish, the physical available area is more than 40 times that of a 15 m reflector such as the SKA dish. Therefore, it is vital with a high aperture efficiency, using as much of the 100 m diameter as possible, to achieve high sensitivity. For a prime-focus reflector, aperture efficiency η_{a}, can be calculated fast with the equations provided in [32], instead of the more time consuming PO+PTD simulation of a 100 m dish. The system simulation can therefore be reduced to a combination of CST and MATLAB that calculate the efficiency during optimization, as was the case in Paper C and Paper D. Antenna noise temperature can be approximated by (2.12). In [24] a proposed QRFH for $f/D = 0.3$ over 4:1 bandwidth

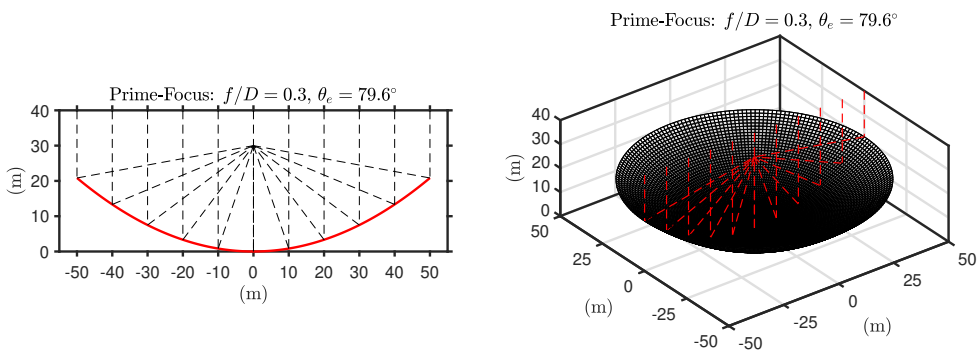

(a) (b)

Fig. 3.15: $f/D = 0.3$ for the Effelsberg 100 m telescope in prime-focus, $\theta_e = 79.6°$. (a) Cross-section view; (b) Perspective view.

has an expected aperture efficiency of 40–45%. The 7:1 QRFH proposed in the same reference has a minimum $\eta_{\mathrm{a}} = 35\%$. In Paper C and Paper D the expected aperture

efficiency of the dieletrically loaded QRFH is above 50% in average with a minimum of 44% over 10:1 bandwidth. The dielectric improves the QRFH beamwidth consistency in H-plane ($\phi = 90°$) over frequency, as shown in Fig. 6 of Paper D. The dielectric load has a broadening effect on the beam for mid and upper frequency range. This is confirmed by looking at the simulated intensity of the E–field component along the co-polarization axis in E- and H-plane, shown below for 15 GHz in Fig. 3.16. There is almost no effect in E-plane (see Fig. 3.16b), but in H-plane the intesity is spread at a wider angle when the dielectric load is installed (see Fig. 3.16d). This improves the illumination of the reflector as well as the phase efficiency at mid and upper frequencies. In Paper D, it is shown that the suggested approach of dielectrically loading the QRFH improves phase efficiency to a high, near-constant, level over decade bandwidth. The cross-polarization is also improved for mid and upper frequencies by the dielectric load. The performance at the lower frequency range is mostly determined by the QRFH's metallic structure. The feed's polarization purity on the reflector is represented by the intrinsic cross-polarization ratio (IXR) [35]. For the SKA, minimum IXR should be better than 15 dB within HPBW. For the dielectrically loaded QRFH, this is achieved for most of the band in the unshaped prime-focus reflector, as shown in Fig. 12 of Paper D.

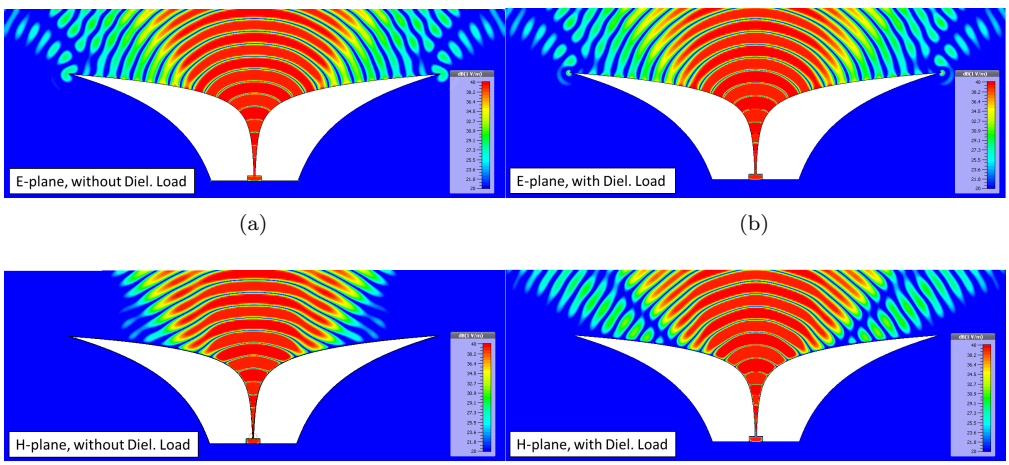

(a) (b)

(c) (d)

Fig. 3.16: Intensity for the co-polarized component of the E-field at 15 GHz. (a) E-plane, without dielectric load; (b) E-plane, with dielectric load; (c) H-plane, without dielectric load; (d) H-plane, with dielectric load.

3.5.2 Shaped dielectric load - beyond decade bandwidth

Dielectric loading could potentially extend the QRFH performance beyond decade bandwidth. Simulated results in Fig. 3.18 over 13:1 bandwidth are normalized to the lowest frequency of the band, ν_{min}. These preliminary results are obtained by slightly shaping

the dielectric, meaning that it is not a pure cylinder type structure, but more similar to a cone. The low-profile and low-loss material is kept consistent, and the structure could still be manufactured with CNC machining. Simulated aperture efficiency in a f/D=0.3 prime-focus reflector is better than 40% across the band, with high spill-over efficiency and phase efficiency, as shown in Fig. 3.18a. The same design is also evaluated for efficiency and IXR in the SKA dish. With the dielectric load, the IXR of mid and upper frequencies in the SKA dish (Fig. 3.18b) is comparable to those of the SKA Band 1 QRFH. The 13:1 bandwidth could cover SKA Band 3 through 5 and beyond, with one single feed over ∼1.7–20 GHz. The adaptability of the QRFH and the simple dielectric structure, could provide an interesting UWB design after further optimization for this application. Once the 3D-printing technology achieves high accuracy with low cost for the most common dielectrics, any potential shape can be realized. This is similar to the expectation for lens-antenna research.

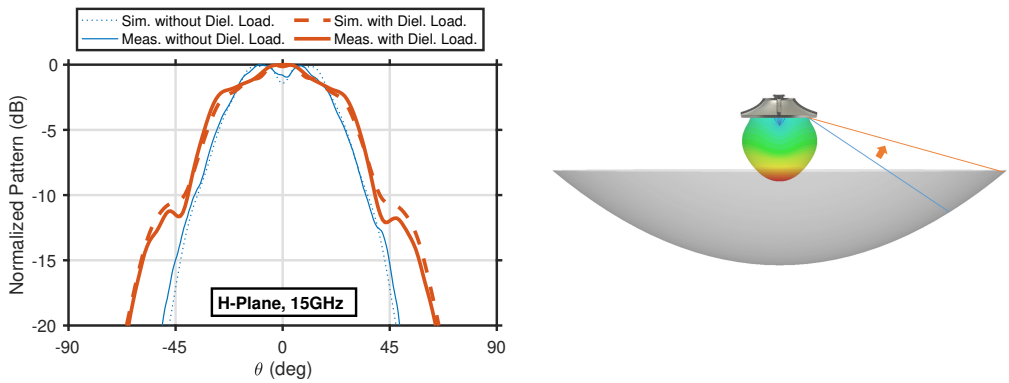

(a) (b)

Fig. 3.17: (a) Co-polarization beam pattern in H-plane at 15 GHz, for a QRFH simulated and measured with and without dielectric load. (b) Illustrating the improved illumination from a broader feed beam pattern.

3.5.3 Manufacture and tolerances

For the mechanical realization of QRFHs two approaches are common: 1) The horn structure is lathed in one piece, with separately machined ridges that are screwed into the horn [22]; 2) The horn structure is molded or machined in four quarter-pieces, and the ridges are machined separately. The ridges are then clamped between adjacent sides of the quarters by screws along the horn profile. For the QRFHs presented in Paper A through Paper D the second method has been used with good results. For this method, accurate tolerances at the flat contacting surface of the quarter-pieces are important. The same is then implied for the ridge surface so that accurate alignment is achieved when they are clamped together, as illustrated in Fig. 3.19a. The alignment is crucial to

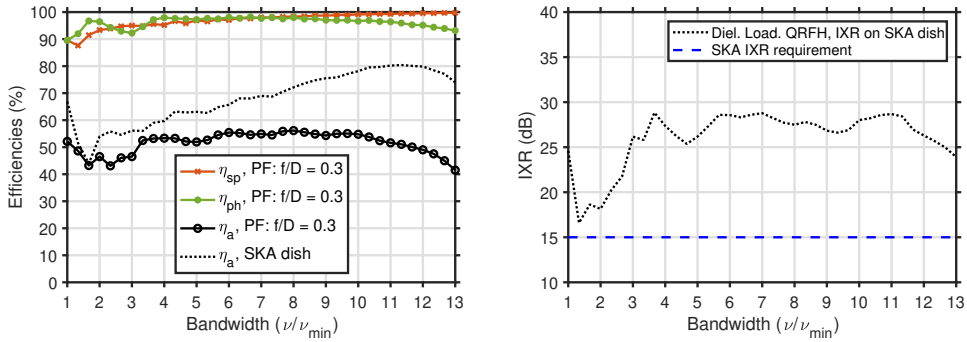

(a) (b)

Fig. 3.18: Dielectrically loading the QRFH can increase performance beyond decade bandwidth, here shown for 13:1 bandwidth. The simulated results are shown for a preliminary design of a slightly shaped dielectric load. Simulated efficiencies (a) compared for axisymmetric prime-focus reflector and the shaped offset Gregorian SKA reflector; In (b) the IXR requirement in the SKA dish is fulfilled over 13:1 bandwidth for this design.

avoid any unwanted mode propagation or impedance mismatch. It is also important to ensure a good electrical contact between ridge and horn along this edge, as illustrated in Fig. 3.19b, to avoid leakage. The surface currents are generally concentrated around the ridges, and separation between the ridge and quarter-piece can degrade the performance. To clamp the quarters and ridge tight, screws are used on the outside with the spacing in between typically chosen such that it is less than $\lambda/4$. The single-ended excitation can

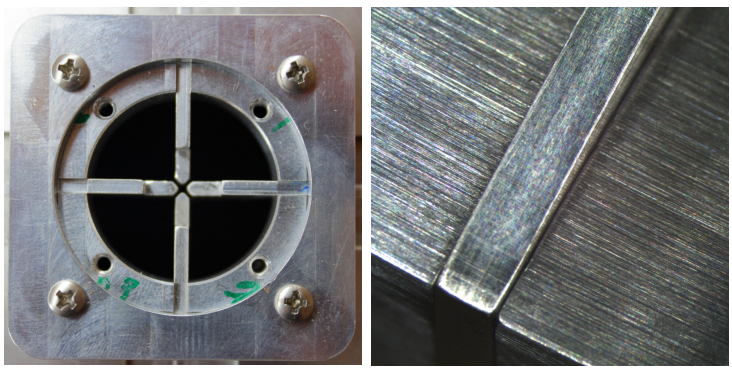

(a) (b)

Fig. 3.19: (a) Ridges aligned by clamping between four quarters, here seen from the back-short of the QRFH with the bottom-lid removed; (b) Zoom-in on ridge-to-flare contact for 2 mm thick ridges.

be performed with a coax launch-pin inserted into a standard, commercially available SMA connector, shown in Fig. 3.20b. The launch-pin is fed through the ridge with either a surrounding dielectric or as an air-coax. For simplicity and low cost, the launch-pin and hole dimensions can be designed so that off-the-shelf products are applicable. In Fig. 3.20c, a launch-pin made from a UT-047 semi-rigid cable is presented for a 50-Ω interface. The launch-pin surrounded by dielectric can suffer from tolerances that vary over length. However, with very small directions the dielectric has an aligning effect that mitigates the risk of short-circuit towards the ridge or the orthogonal launch-pin. The launch-pin is contacted in the opposite ridge with a chuck connector that is pressed from the back by a push-pin and screw. The hole is chamfered from the inside of the ridge so that the chuck clamps around the launch-pin when pushed towards the ridge-hole, illustrated in Fig. 3.20a. For a large QRFH as in Paper A and Paper B, the launch-pin can

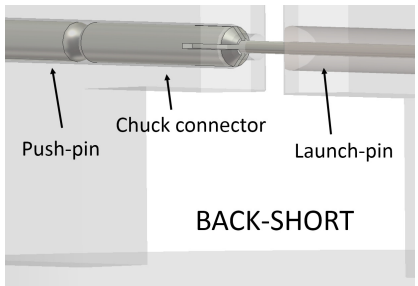

(a)

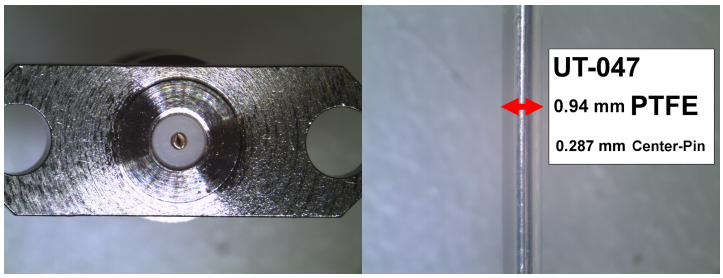

(b) (c)

Fig. 3.20: (a) SMA connector specified up to 27 GHz; (b) "Peeled" semi-rigid UT-047 as launch pin, 0.94 mm Teflon (PTFE), 0.287 mm SPCW pin. (c) Illustration of single-ended launch-pin making contact through a chuck connector to the ridge opposite.

be contacted by screwing it in in place inside the ridges. For higher frequencies the chuck connector has been shown succesful up to 24 GHz [41]. Another approach with a sliding launch-pin that can be soldered into the opposing ridge before assembly has been used up to 50 GHz [43]. It was shown in Paper D how tolerances play a key role to impedance matching at the excitation point of the QRFH. Misalignment in the separation between ridges and the contacting-point of the launch-pin in opposite ridge, can degrade the input reflection coefficient significantly. The port isolation is further degraded by asymmetries

at the excitation point, where an acceptable measured level is better than 35 dB. With a dielectric load in between the ridges, the tolerances of both the dielectric and the ridges are crucial. For any high frequency design, a tolerance analysis should be performed before manufacture. Possible misalignments should simultaneously and randomly be varied over a specific range, for a set of simulations, similar to Monte-Carlo analysis [56]. This approach can predict combined effects from different misalignments, which is most likely the actual situation. For a mass production this is an absolute necessity to predict acceptable variations in manufactured pieces and avoid deviations from specification.

CHAPTER 4

Paper Summary and Future Work

In this chapter a brief summary is given for each of the appended papers. Paper A and Paper B present the 3:1 spline-defined QRFH design for SKA Band 1 over 350–1050 MHz. Paper C and Paper D present the 10:1 dielectrically loaded QRFH design for BRAND EVN over 1.5–15.5 GHz. The future outlook of the work presented in this thesis is given as well.

4.1 Summary of Paper A

In this paper, the first reflector beam pattern measurement for the SKA Band 1 feed package is presented. The feed was installed and tested on the Dish Verification Antenna 1 (DVA1) in Penticton, BC, Canada during 2016 and 2017. The SKA Band 1 feed is a 3:1 bandwidth spline-defined QRFH optimized for high sensitivity on the SKA dish over 350–1050 MHz. The feed package is a complete room temperature system with LNAs mounted directly inside the ridges. The DVA1 is a pre-cursor to the SKA dish, and is a 15 m offset Gregorian reflector with feed-up configuration. With the Band 1 feed installed, the telescope main-lobe was swept over the sun to produce beam cuts at different frequencies. Corrections were applied to the measured results for the sun solid angle, elevation-axis deformation and aperture efficiency. Due to the general RFI pollution at the UHF-band, the three frequency points measured were chosen so that RFI-free bandwidth was available around the center frequency. The measured beam patterns show good agreement with simulations, where the result for the lowest frequency is slightly deviating due to saturation of the receiver chain. To determine the RFI-free frequencies and to confirm the estimated receiver noise temperature, the feed package's Y-factor was measured in the hot-cold-test-facility. The measured receiver noise is in good agreement with the estimated model.

4.2 Summary of Paper B

In this paper, the first measured sensitivity levels for the SKA Band 1 feed package are presented. The feed was installed on a 13.5 m MeerKAT reflector in the Karoo desert, South Africa. The SKA Band 1 feed is a 3:1 bandwidth spline-defined QRFH optimized for high sensitivity on the SKA dish over 350–1050 MHz. The feed package is a complete room temperature system with LNAs mounted directly inside the ridges. The sensitivity was measured through drift scans of the known sources Orion A and Hydra A. To account

for the difference in brightness temperature near these sources compared to the general SKA model, corrections were applied. Corrections were also applied for the difference in projected aperture of the ideal reflector model of MeerKAT compared to the slightly larger mechanical model that was constructed. Aperture efficiency was measured using microwave holography and the IXR was calculated using measured reflector beam patterns. Good agreement between simulated and measured results were found which validates the system simulation. This gives confidence that the SKA Band 1 feed package will perform according to specification once it is installed on the first SKA dish that currently is being built in South Africa.

4.3 Summary of Paper C

In this paper, development to improve QRFH decade bandwidth through dielectric loading is presented. The BRAND project aims to cover L-,S-,C-,X- and Ku-band with one receiver system and a single feed. The first prototype is developed for the Effelsberg 100 m prime-focus with f/D=0.3. The simulated average aperture efficiency is 50 % and the input reflection coefficient less than -10 dB over 1.5–15.5 GHz. The optimization scheme and approach of Analytic-Spline-Hybrid (ASH) profiles for QRFHs are also introduced. This entails a combination of analytic and spline-defined profiles to customize the feed shape and performance, and to reduce optimization time compared to a pure spline-profile.

4.4 Summary of Paper D

In this paper, the design, manufacture and measurement of a dielectrically loaded QRFH over decade bandwidth is presented. The feed covers 1.5–15.5 GHz and was designed for an axisymmetric prime-focus reflector with f/D = 0.3. The dielectric load improves the H-plane beamwidth control over frequency for the QRFH, which is confirmed with measurements of the beam pattern. Simulated on an f/D = 0.3 reflector, the phase efficiency is high and near-constant over the decade bandwidth together with a spill-over efficiency better than 90% for 92% of the band. The dielectric load also improves IXR for mid and upper frequencies to a level acceptable for the SKA. SEFD for the proposed QRFH is calculated for a 100 m telescope including blockage from sub-reflector and struts. Receiver noise is based on data from state-of-the-art LNA and receiver components. The simplicity and low-profile of the dielectric load does not alter the QRFH footprint and keeps the system complexity low for integration in a cryostat dewar. The dielectric load is made from low-loss PTFE in the shape of a cylinder which makes it possible to manufacture through standard CNC machining. The QRFH is designed for dual-linear polarization, each with a single-ended 50 Ω interface. The simulated input reflection coefficient is less than -10 dB under nominal tolerance assumption. The measured prototype does not achieve this and an explanation for the deviation is presented with a tolerance analysis of the most critical parameters of the QRFH excitation point.

4.5 Future work

The spline-defined QRFH work has proven very succesful for high-sensitivity design for the SKA project. The final confirmation of the predicted performance for the SKA Band 1 feed package will be received in the near future when the first SKA prototype dish is inaugurated for testing in South Africa. For the SKA Band 1 feed package, which recently passed the critical design review, the SKA dish test is the final milestone before mass production. The approach to use spline-defined profiles of the QRFH has proven useful in other applications as well. The high-frequency SKA Band B feed over 4.6–24 GHz developed for the SKA advanced instrumentation programme, achieves excellent performance over 5.2:1 bandwidth [41]. For the ngVLA, the spline-defined profiles have been used in a demonstrator QRFH with 3.5:1 bandwidth as part of the pre-proposal work [57]. For similar applications, the Analytic-Spline-Hybrid (ASH) approach should be explored further for different bandwidths and reflector geometries.

For the dielectrically loaded QRFH, more work should be done to improve the cross-polar level at low frequencies. Possibly a simplified choke-skirt as in [50] could be implemented if more complexity is allowed. The BRAND QRFH prototype over 1.5–15.5 GHz will be integrated with cryogenic LNAs and tested in a dewar during the next phase. Eventually the whole receiver chain of BRAND will be tested on the Effelsberg telescope with expected VLBI results in 2020. The approach to shape dielectrics could improve the performance even more, and extend the bandwidth beyond 10:1. With the evolution of 3D-printing in material such as Teflon (PTFE), more advanced shapes could be explored. Due to the simple approach of clamping the dielectric load between the ridges, it can be replaced easily if an improved shape is found.

Both the SKA Band B and BRAND QRFH have shown interesting performance in the VGOS Gregorian ring-focus system for geodetic VLBI [58], [59]. The SKA Band B feed includes the water-vapor line at 22 GHz which could make line-of-sight water-vapor radiometry possible in parallel while observing [58].

The study of bandwidth trade-offs for sensitivity and aperture efficiency introduced in [59] needs further investigation for different reflector geometries, and other state-of-the-art UWB feeds. This study has not been included in this thesis, however the designs presented are relevant for that future work.

References

[1] J. W. M. Baars, *The Paraboloidal Reflector Antenna in Radio Astronomy and Communication: Theory and Practice*, ser. Astrophysics and Space Science Library. Springer New York, 2007, ISBN: 9780387697345.

[2] T. L. Wilson, K. Rohlfs, and S. Hüttemeister, *Tools of Radio Astronomy*, 6th Edition, A. Library and Astrophysics, Eds. Springer, 2013, ISBN: 9783642399497.

[3] M. De Vos, A. W. Gunst, and R. Nijboer, "The LOFAR telescope: System architecture and signal processing", *Proceedings of the IEEE* vol. 97, no. 8 2009, pp. 1431–1437, 2009, ISSN: 00189219. DOI: 10.1109/JPROC.2009.2020509.

[4] P. S. Kildal, L. A. Baker, and T. Hagfors, "The Arecibo Upgrading: Electrical Design and Expected Performance of the Dual-Reflector Feed System", *Proceedings of the IEEE* vol. 82, no. 5 1994, pp. 714–724, 1994, ISSN: 15582256. DOI: 10.1109/5.284738.

[5] D. Li, R. Nan, Z. Pan, C. Jin, L. Zhu, Q. Wang, P. Jiang, K. Xu, and C. Li, "The Five-hundred-meter Aperture Spherical Radio Telescope (FAST) project", in *International Topical Meeting on Microwave Photonics (MWP 2015)*, Paphos, Cyprus: IEEE, Oct. 2015. DOI: 10.1002/2015RS005877.

[6] A. L. Fey, D. Gordon, C. S. Jacobs, C. Ma, R. A. Gaume, E. F. Arias, G. Bianco, D. A. Boboltz, S. Böckmann, S. Bolotin, P. Charlot, A. Collioud, G. Engelhardt, J. Gipson, A. M. Gontier, R. Heinkelmann, S. Kurdubov, S. Lambert, S. Lytvyn, D. S. MacMillan, Z. Malkin, A. Nothnagel, R. Ojha, E. Skurikhina, J. Sokolova, J. Souchay, O. J. Sovers, V. Tesmer, O. Titov, G. Wang, and V. Zharov, "The second realization of the international celestial reference frame by very long baseline interferometry", *Astronomical Journal* vol. 150, no. 2 2015, 2015, ISSN: 00046256. DOI: 10.1088/0004-6256/150/2/58.

[7] A. E. Niell, A. R. Whitney, B. Petrachenko, W. Schlüter, N. R. Vandenberg, H. Hase, Y. Koyama, M. C., H. Schuh, and G. Tuccari, "VLBI2010: Current and future requirementsfor geodetic VLBI systems (WG3—final report)", In 2005 IVS Annual Report NASA/TP-2006-214136. International VLBI Service for Geodesy and Astrometry (IVS), 2005. [Online]. Available: https://ivscc.gsfc.nasa.gov/about/wg/wg3/IVS_WG3_report_050916.pdf.

[8] B. Petrachenko, A. Niell, D. Behrend, B. Corey, J. Böhm, P. Charlot, A. Collioud, J. Gipson, R. Haas, T. Hobiger, Y. Koyama, D. MacMillan, Z. Malkin, T. Nilsson, A. Pany, G. Tuccari, A. Whitney, and J. Wresnik., "Design Aspects of the VLBI2010 System", In Progress Report of the IVS VLBI2010 Commitee, NASA/TM-2009-214180, 2009. [Online]. Available: https://ntrs.nasa.gov/search.jsp?R=20090034177.

[9] G. Elgered, R. Haas, J. Conway, R. Hammargren, L. Helldner, T. Hobiger, M. Pantaleev, and L. Wennerbäck, "The Onsala Twin Telescopes Project", in *Proc. 23rd Working Meeting of the Euro. Very Long Baseline Interferometry Group for Geodesy and Astrometry (EVGA 2017)*, EVGA, 2017.

[10] R. Lehmensiek and I. P. Theron, "L-band feed horn and orthogonal mode transducer for the KAT-7 radio telescope", *IEEE Trans. Antennas Propag.* vol. 59, no. 6 Jun. 2011, pp. 1894–1901, Jun. 2011, ISSN: 0018926X. DOI: 10.1109/TAP.2011.2122217.

[11] M. McKinnon, C. Carilli, and T. Beasley, "The next generation very large array", in *Proc. SPIE*, vol. 9906, Jul. 2016, p. 990 627, ISBN: 9781510601918. DOI: 10.1117/12.2234941.

[12] W. J. Welch, M. Fleming, C. Munson, J. Tarter, G. R. Harp, R. Spencer, and N. Wadefalk, "New cooled feeds for the allen telescope array", *Publ. Astro. Soc. Pacific* vol. 129, no. 974 Mar. 2017, Mar. 2017, ISSN: 00046280. DOI: 10.1088/1538-3873/aa5d4f.

[13] I. P. Theron, R. Lehmensiek, and D. I. L. de Villiers, "The design of the MeerKAT dish optics", in *Proc. Int. Conf. Electromagn. Advanced Appl. (ICEAA 2012)*, Sep. 2012, pp. 539–542, ISBN: 9781467303354. DOI: 10.1109/ICEAA.2012.6328685.

[14] P. E. Dewdney, W. Turner, R. Millenaar, R. McCool, J. Lazio, and T. J. Cornewell, "SKA1 System Baseline Design (SKA-TEL-SKO-DD-001)", SKA Organisation, Mar. 2013. [Online]. Available: https://www.skatelescope.org/wp-content/uploads/2012/07/SKA-TEL-SKO-DD-001-1%5C_BaselineDesign1.pdf.

[15] J. Schleeh, N. Wadefalk, P. A. Nilsson, J. P. Starski, G. Alestig, J. Halonen, B. Nilsson, A. Malmros, H. Zirath, and J. Grahn, "Cryogenic 0.5-13 GHz low noise amplifier with 3 K mid-band noise temperature", in *IEEE MTT-S Int. Microw. Symp. Dig. (IMS 2012)*, Montreal, QC, Canada, 2012, pp. 15–17, ISBN: 9781467310871. DOI: 10.1109/MWSYM.2012.6259542.

[16] J. Schleeh, G. Moschetti, N. Wadefalk, E. Cha, A. Pourkabirian, G. Alestig, J. Halonen, B. Nilsson, P. Nilsson, and J. Grahn, "Cryogenic LNAs for SKA band 2 to 5", in *IEEE MTT-S Int. Microw. Symp. Digest (IMS 2017)*, Honolulu, HI, USA, Jun. 2017, pp. 164–167, ISBN: 9781509063604. DOI: 10.1109/MWSYM.2017.8058948.

[17] N. Wadefalk, P.-S. Kildal, and H. Zirath, "A low noise integrated 0.3-16 GHz differential amplifier for balanced ultra wideband antennas", in *Tech. Dig. IEEE Compound Semicond. Integrated Circuit Symp. (CSIC 2010)*, 2010, pp. 3–6, ISBN: 9781424474387. DOI: 10.1109/CSICS.2010.5619677.

[18] A. H. Akgiray, S. Weinreb, R. Leblanc, M. Renvoise, P. Frijlink, R. Lai, and S. Sarkozy, "Noise measurements of discrete HEMT transistors and application to wideband very low-noise amplifiers", *IEEE Trans. Microw. Theory Techn.* vol. 61, no. 9 2013, pp. 3285–3297, 2013, ISSN: 00189480. DOI: 10.1109/TMTT.2013.2273757.

[19] J. Yang, M. Pantaleev, P.-S. Kildal, B. Klein, Y. Karandikar, L. Helldner, N. Wadefalk, and C. Beaudoin, "Cryogenic 2-13 GHz eleven feed for reflector antennas in future wideband radio telescopes", *IEEE Trans. Antennas Propag.* vol. 59, no. 6 Jun. 2011, pp. 1918–1934, Jun. 2011, ISSN: 0018926X. DOI: 10.1109/TAP.2011.2122229.

[20] J. Yang, M. Pantaleev, P.-S. Kildal, and L. Helldner, "Design of compact dual-polarized 1.2-10 GHz eleven feed for decade bandwidth radio telescopes", *IEEE Trans. Antennas Propag.* vol. 60, no. 5 May 2012, pp. 2210–2218, May 2012, ISSN: 0018926X. DOI: 10.1109/TAP.2012.2189732.

[21] G. Cortes-Medellin, "Non-planar quasi-self-complementary ultra-wideband feed antenna", *IEEE Trans. Antennas Propag.* vol. 59, no. 6 Jun. 2011, pp. 1935–1944, Jun. 2011, ISSN: 0018926X. DOI: 10.1109/TAP.2011.2122226.

[22] A. Akgiray, S. Weinreb, W. A. Imbriale, and C. Beaudoin, "Circular quadruple-ridged flared horn achieving near-constant beamwidth over multioctave bandwidth: Design and measurements", *IEEE Trans. Antennas Propag.* vol. 61, no. 3 Mar. 2013, pp. 1099–1108, Mar. 2013, ISSN: 0018926X. DOI: 10.1109/TAP.2012.2229953.

[23] T. S. Beukman, P. Meyer, M. V. Ivashina, and R. Maaskant, "Modal-based design of a wideband quadruple-ridged flared horn antenna", *IEEE Trans. Antennas Propag.* vol. 64, no. 5 May 2016, pp. 1615–1626, May 2016, ISSN: 0018926X. DOI: 10.1109/TAP.2016.2537363.

[24] A. H. Akgiray, "New technologies driving decade-bandwidth radio astronomy : quad-ridged flared horn and compound-semiconductor LNAs", PhD thesis, California Institute of Technology (Caltech), 2013. [Online]. Available: http://thesis.library.caltech.edu/7644/.

[25] T. S. Beukman, "Modal-Based Design Techniques for Circular Quadruple-Ridged Flared Horn Antennas", PhD thesis, Stellenbosch University, 2015. [Online]. Available: http://hdl.handle.net/10019.1/96948.

[26] G. Tuccari, W. Alef, M. Pantaleev, **J. Flygare**, J. A. López Pérez, J. A. López Fernández, G. Schonderbeek, and V. Bezrukos, "BRAND: A very wide-band receiver for the EVN", in *Proc. 23rd Working Meeting of the Euro. Very Long Baseline Interferometry Group for Geodesy and Astrometry (EVGA 2017)*, Gothenburg, Sweden, May 2017, pp. 81–83.

[27] C. A. Balanis, *Modern Antenna Handbook*. New York, NY, USA: Wiley-Interscience, 2008, ISBN: 0470036346, 9780470036341.

[28] P.-S. Kildal, *Foundations of Antennas - A Unified Approach for Line-Of-Sight and Multipath*. 2014, ISBN: 9789004310087. DOI: 10.15713/ins.mmj.3.

[29] D. M. Pozar, *Microwave Engineering*. Wiley, 2012, ISBN: 9780470631553.

[30] C. A. Balanis, *Antenna Theory: Analsysi and Design*. New York, NY, USA: Wiley-Interscience, 2005, ISBN: 0471714623.

[31] IEEE, "IEEE Standard for Definitions of Terms for Antennas (IEEE Std 145)", IEEE Antennas and Propagation Society, Tech. Rep., 2013. DOI: 10.1109/IEEESTD.2014.6758443.

[32] P.-S. Kildal, "Factorization of the feed Efficiency of Paraboloids and Cassegrain Antennas", *IEEE Trans. Antennas Propag.* vol. 33, no. 8 1985, pp. 903–908, 1985, ISSN: 15582221. DOI: 10.1109/TAP.1985.1143689.

[33] G. Cortes-Medellin, "MEMO 95 Antenna noise temperature calculation", SKA Memo, Jul. 2007, pp. 1–13. [Online]. Available: https://www.skatelescope.org/uploaded/6967%5C_Memo%5C_95.pdf.

[34] R. Lehmensiek, I. P. Theron, and D. I. De Villiers, "Deriving an Optimum Mapping Function for the SKA-Shaped Offset Gregorian Reflectors", *IEEE Trans. Antennas Propag.* vol. 63, no. 11 2015, pp. 4658–4666, 2015, ISSN: 0018926X. DOI: 10.1109/TAP.2015.2477408.

[35] T. D. Carozzi and G. Woan, "A fundamental figure of merit for radio polarimeters", *IEEE Trans. Antennas Propag.* vol. 59, no. 6 Jun. 2011, pp. 2058–2065, Jun. 2011, ISSN: 0018926X. DOI: 10.1109/TAP.2011.2123862. arXiv: 0908.2330.

[36] S. B. Cohn, "Properties of Ridge Wave Guide", *Proceedings of the IRE* vol. 35, no. 8 1947, pp. 783–788, 1947, ISSN: 00968390. DOI: 10.1109/JRPROC.1947.226277.

[37] S. Hopfer, "The Design of Ridged Waveguides", *IRE Transactions on Microwave Theory and Techniques* vol. 3, no. 5 1955, pp. 20–29, 1955, ISSN: 00972002. DOI: 10.1109/TMTT.1955.1124972.

[38] M. H. Chen, G. N. Tsandoulas, and F. G. Willwerth, "Modal Characteristics of Quadruple-Ridged Circular and Square Waveguides", *IEEE Trans. Microw. Theory Techn.* vol. 22, no. 8 1974, pp. 801–804, 1974, ISSN: 15579670. DOI: 10.1109/TMTT.1974.1128341.

[39] A. Akgiray, S. Weinreb, and W. A. Imbriale, "The quadruple-ridged flared horn : A flexible multi-octave reflector feed spanning f/0.3 to f/2.5", in *Proc. 7th Euro. Conf. Antennas Propag. (EuCAP 2013)*, Gothenburg, Sweden: IEEE, 2013, pp. 768–769, ISBN: 9788890701818. [Online]. Available: https://ieeexplore.ieee.org/document/6546381.

[40] A. Akgiray and S. Weinreb, "Ultrawideband square and circular quad-ridge horns with near-constant beamwidth", in *Proc. IEEE International Conference on Ultra-Wideband*, Syracuse, NY, USA: IEEE, 2012, pp. 518–522, ISBN: 9781457720307. DOI: 10.1109/ICUWB.2012.6340506.

[41] B. Dong, J. Yang, J. Dahlström, **J. Flygare**, M. Pantaleev, and B. Billade, "Optimization and Realization of Quadruple-ridge Flared Horn with New Spline-defined Profiles as a High-efficiency Feed for Reflectors over 4.6 - 24 GHz", *IEEE Trans. Antennas Propag., Accepted for publication Sep. 2018*,

[42] B. Billade, **J. Flygare**, M. Dahlgren, B. Wästberg, and M. Pantaleev, "A wide-band feed system for SKA band 1 covering frequencies from 350 - 1050 MHz", in *Proc. 10th Euro. Conf. Antennas Propag. (EuCAP 2016)*, Davos, Switzerland, Apr. 2016, ISBN: 9788890701863. DOI: 10.1109/EuCAP.2016.7481794.

[43] J. Shi, S. Weinreb, W. Zhong, X. Yin, and M. Yang, "Quadruple-Ridged Flared Horn Operating From 8 to 50 GHz", *IEEE Trans. Antennas Propag.* vol. 65, no. 12 Dec. 2017, pp. 7322–7327, Dec. 2017. DOI: 10.1109/TAP.2017.2760365.

[44] J. Kennedy and R. Eberhart, "Particle swarm optimization", in *Proc. IEEE International Conference on Neural Networks (ICNN 2015)*, Perth, WA, Australia: IEEE, 1995, pp. 1942–1948, ISBN: 0-7803-2768-3. DOI: 10.1016/0040-1951(89)90193-5. arXiv: arXiv:1011.1669v3.

[45] M. V. Ivashina, O. Iupikov, R. Maaskant, W. A. Van Cappellen, and T. Oosterloo, "An optimal beamforming strategy for wide-field surveys with phased-array-fed reflector antennas", *IEEE Trans. Antennas Propag.* vol. 59, no. 6 2011, pp. 1864–1875, 2011, ISSN: 0018926X. DOI: 10.1109/TAP.2011.2123865.

[46] G. H. Tan, R. Lehmensiek, B. Billade, K. Caputa, S. Gauffre, I. P. Theron, M. Pantaleev, Z. Ljusic, B. Quertier, and A. Peens-Hough, "An innovative, highly sensitive receiver system for the Square Kilometre Array Mid Radio Telescope", vol. 9906, no. 0 2016, p. 990 660, 2016, ISSN: 1996756X. DOI: 10.1117/12.2230897. [Online]. Available: http://proceedings.spiedigitallibrary.org/proceeding.aspx?doi=10.1117/12.2230897.

[47] W. A. Imbriale, "Faster antenna noise temperature calculations using a novel approximation technique", in *IEEE International Symposium on Antennas and Propagation and CNC-USNC/URSI Radio Science Meeting (APSURSI 2010)*, 2010, ISBN: 9781424449682. DOI: 10.1109/APS.2010.5562198.

[48] D. I. De Villiers and R. Lehmensiek, "Rapid calculation of antenna noise temperature in offset gregorian reflector systems", *IEEE Trans. Antennas Propag.* vol. 63, no. 4 2015, pp. 1564–1571, 2015, ISSN: 0018926X. DOI: 10.1109/TAP.2015.2399933.

[49] D. G. Bodnar, "Standard Gain Horn Computations Versus Measured Data", in *14th International Symposium on Antenna Technology and Applied Electromagnetics & the American Electromagnetics Conference*, Ottawa, ON, Canada: IEEE, 2010, ISBN: 9781424450503.

[50] A. Dunning, M. Bowen, M. Bourne, D. Hayman, and S. L. Smith, "An ultra-wideband dielectrically loaded quad-ridged feed horn for radio astronomy", in *Proc. IEEE-APS Conf. Antennas Propag. Wireless Communic. (APWC 2015)*, Turin, Italy, Sep. 2015, pp. 787–790, ISBN: 9781479978090. DOI: 10.1109/APWC.2015.7300180.

[51] D. M. Pozar and B. Kaufman, "Comparison of Three Methods for the Measurement of Printed Antenna Efficiency", *IEEE Transactions on Antennas and Propagation* vol. 36, no. 1 1988, pp. 136–139, 1988, ISSN: 15582221. DOI: 10.1109/8.1084.

[52] J. Schleeh, N. Wadefalk, P. A. Nilsson, and J. Grahn, "10 K room temperature LNA for SKA band 1", in *IEEE MTT-S Int. Microw. Symp. Dig. (IMS 2016)*, San Francisco, CA, USA, Aug. 2016, ISBN: 9781509006984. DOI: 10.1109/MWSYM.2016.7540344.

[53] W. D. Burnside and C. W. Chuang, "An Aperture-Matched Horn Design", *IEEE Trans. Antennas Propag.* vol. 30, no. 4 1982, pp. 790–796, 1982, ISSN: 15582221. DOI: 10.1109/TAP.1982.1142850.

[54] A. Akgiray, S. Weinreb, and W. Imbriale, "Design and measurements of dual-polarized wideband constant-beamwidth quadruple-ridged flared horn", in *IEEE Antennas and Propagation Society, AP-S International Symposium (Digest)*, IEEE, 2011, pp. 1135–1138, ISBN: 9781424495634. DOI: 10.1109/APS.2011.5996483.

[55] R. J. Bauerle, R. Schrimpf, E. Gyorko, and J. Henderson, "The Use of a Dielectric Lens to Improve the Efficiency of a Dual-Polarized Quad-Ridge Horn From 5 to 15 GHz", *IEEE Trans. Antennas Propag.* vol. 57, no. 6 2009, pp. 1822–1825, 2009.

[56] A. Algaba Brazalez, **J. Flygare**, J. Yang, V. Vassilev, M. Baquero-Escudero, and P.-S. Kildal, "Design of F-Band Transition from Microstrip to Ridge Gap Waveguide Including Monte Carlo Assembly Tolerance Analysis", *IEEE Trans. Microw. Theory Techn.* vol. 64, no. 4 Apr. 2016, pp. 1245–1254, Apr. 2016, ISSN: 00189480. DOI: 10.1109/TMTT.2016.2535334.

[57] S. Weinreb, H. Mani, W. Zhong, **J. Flygare**, B. Billade, A. Akgiray, and L. Dong, "Cryogenic 1.2 to 116 GHz Receiver for Large Arrays", in *Proc. 12th Euro. Conf. Antennas Propag. (EuCAP 2018)*, London, UK, Apr. 2018.

[58] **J. Flygare**, M. Pantaleev, J. Conway, M. Lindqvist, L. Helldner, M. Dahlgren, and P. Forkman, "Ultra-wideband feed systems for the EVN and SKA - evaluated for VGOS", in *Proc. 10th General Meeting, International VLBI Service for Geodesy and Astrometry (IVS 2018)*, Longyearbyen, Svalbard, Norway, Jun. 2018.

[59] **J. Flygare**, M. Pantaleev, J. Conway, and M. Lindqvist, "Design trade-offs in feed systems for ultra-wideband VLBI observations", in *Proc. 10th General Meeting, International VLBI Service for Geodesy and Astrometry (IVS 2018)*, Longyearbyen, Svalbard, Norway, Jun. 2018.